Towards Verifiable Adaptive Control for Safety Critical Applications

by

Mac Schwager

B.S., Mechanical Engineering
Stanford University, 2000

Submitted to the Department of Mechanical Engineering
in partial fulfillment of the requirements for the degree of

Master of Science in Mechanical Engineering

at the

MASSACHUSETTS INSTITUTE OF TECHNOLOGY

June 2005

Author .....
Department of Mechanical Engineering
June 1, 2005

Certified by .....
Anuradha M. Annaswamy
Senior-Research Scientist
Thesis Supervisor

Accepted by .....
Lallit Anand
Professor of Mechanical Engineering
Chairman, Department Committee on Graduate Students

Towards Verifiable Adaptive Control for Safety Critical Applications

by

Mac Schwager

B.S., Mechanical Engineering

Stanford University, 2000

Submitted to the Department of Mechanical Engineering
on June 1, 2005, in partial fulfillment of the
requirements for the degree of
Master of Science in Mechanical Engineering

Abstract

To be implementable in safety critical applications, adaptive controllers must be shown to behave strictly according to predetermined specifications. This thesis presents two tools for verifying specifications relevant to practical direct-adaptive control systems. The first tool is derived from an asymptotic analysis of the error dynamics of a direct adaptive controller and uncertain linear plant. The analysis yields a so called Reduced Linear Asymptotic System, which can be used for designing adaptive systems to meet transient specifications. The tool is demonstrated in two design examples from flight mechanics, and verified in numerical simulation. The second tool developed is an algorithm for direct-adaptive control of plants with magnitude saturation constraints on multiple inputs. The algorithm is a non-trivial extension of an existing technique for single input systems with saturation. Boundeness of all signals is proved for initial conditions in a compact region. In addition, the notion of a class of multi-dimensional saturation functions is introduced. The saturation compensation technique is demonstrated in numerical simulation. Finally, these tools are applied to design a direct-adaptive controller for a realistic multi-input aircraft model to accomplish control reconfiguration in the case of unforseen failure, damage, or disturbances. A novel control design for incorporating control allocation and reconfiguration is introduced. The adaptive system is shown in numerical simulation to have favorable transient qualities and to give a stable response with input saturation constraints.

Thesis Supervisor: Anuradha M. Annaswamy
Title: Senior Research Scientist

Acknowledgments

I thank my advisor, Dr. Anuradha M. Annaswamy, for her continual motivation and teaching. All that I know about the practice of mathematics I have learned from her. I am grateful to Dr. Eugene Lavretsky for many lively conversations and for his perceptive insights into flight mechanics. I also owe thanks to Boeing's Strategic University Initiative and the Army Research Office for financial support. Finally, I thank Tana and my mother, without whose loving encouragement I never would have completed this project.

Contents

List of Figures

List of Tables

Chapter 1

Introduction

This work is to be considered an initial step toward developing a set of tools and procedures that can be used for designing practical adaptive controllers for systems in which safety and reliability are critical operating requirements. In the past, adaptive control has been limited to applications without stringent safety requirements such as high performance specialized robotics applications, or docile industrial control applications. Safety critical applications demand that controllers behave strictly according to predetermined specifications. Unfortunately, the inherently nonlinear nature of adaptive controllers makes them impervious to the analysis techniques relevant to linear controllers. Consequently, the behavior of adaptive controllers in realistic situations involving input disturbances, sensor noise, model structure uncertainty, and input saturation is difficult to characterize. Not only do we lack the means by which to verify that an adaptive controller meets specifications, but it is unclear even how such specifications ought to be posed. It is hoped that this thesis will address both of these problems to some extent.

Two tools are presented in this thesis for the verification of adaptive systems. The tools were developed with two overarching considerations

i) they should be analytically verified, and

ii) they should be practically useful for control design engineers.

The tools are introduced with a theoretical motivation. They are then demonstrated

in several realistic design exercises involving aircraft control. The first tool we derive, the Reduced Linear Asymptotic System (RLAS), provides a means by which to estimate the asymptotic oscillatory properties of an adaptive system. The RLAS leads to a simple design and verification procedure to systematically produce adaptive controllers according to standard transient specifications. The second tool we derive allows for stable adaptive control of plants with saturation constraints on multiple inputs. A previous result for single input adaptive systems [20] is generalized to the multi-input case, which is relevant to many safety critical applications.

1.1 Aircraft Control: An Archetypal Example

Aircraft control was chosen to serve as a backdrop to the theories and techniques presented in this thesis. The application of adaptive control to aircraft promises benefits in safety and robustness and is considered to be one of the main enabling technologies for Unmanned Air Vehicles (UAV's). Early attempts at adaptive flight control used controllers with unproven stability properties, sometimes with disastrous consequences; for example the fatal crash of the NASA X-15 in November, 1967. As a result, much of the theoretical work up to the present time has been rightly focused on stability of adaptive architectures. Currently, there exists an assortment of stable adaptive control strategies, as well as techniques for preserving stability in the presence of unknown, bounded disturbances [27, 34]. In addition, recent military interest in UAV's has caused a surge of adaptive flight control research. UAV's provide an exciting test ground for experimental control techniques. It is reasonable to expect that the viability of adaptive flight control systems must be proven in unmanned vehicles prior to their implementation in manned aircraft, where safety is a much more critical consideration. For this reason, the development of stable and robust adaptive flight control systems for UAV's is a crucial gateway to the broader acceptance of adaptive control strategies for other safety critical applications.

Three common adaptive architectures have been investigated in conjunction with aircraft control. Perhaps the most promising architecture is direct adaptive control,

in which control parameters are adapted based on some performance error. Direct adaptive strategies were explored in [40, 2, 21, 37]. Another common adaptive control architecture, indirect adaptive control, uses a controller derived from a plant model, while the model is continuously updated using system identification techniques. A notable application of an indirect adaptive flight controller is treated in [4] using a multiple model approach. Finally, neural network based flight controllers have also been a popular topic of research [7, 16]. Such controllers use one or more networks of basis functions, which are adapted online using learning algorithms. Each of these control techniques has been investigated in myriad embodiments and variations. In addition, methods such as Training Signal Hedging (TSH) have been developed to overcome the real-world problem of saturating actuators [20, 32, 23]. In [33], TSH was used to develop a direct-adaptive controller for simultaneous control allocation and reconfiguration. Based on this substantial body of research, it can be argued that the study of adaptive flight control systems has reached sufficient maturity to warrant research into more practical problems of integrating adaptive controllers with aircraft systems.

1.2 Verifiable Transient Properties

Currently, one practical obstacle to transitioning adaptive flight controllers into aerospace applications is an inability to analytically assert that the closed-loop system will have acceptable transient behavior. As discussed previously, this is not a trivial task because the dynamics of an adaptive system in closed loop are nonlinear. For example, there is currently no simple analytical technique to determine whether or not a control signal produced by a given adaptive controller will exceed the bandwidth of control actuators. Similarly, there is no simple technique to determine whether or not the response of a given adaptive control system will produce frequencies that may interact with, for instance, unmodeled structural modes. Such concerns can be grouped under the umbrella of Verification and Validation (V&V) and are obviously of paramount importance in application to aircraft and other safety critical systems. However these

concerns have received curiously little attention in the adaptive control literature. Researchers have generally relied on extensive simulation and trial and error to produce adaptive control systems with suitable transient properties.

The V&V techniques that are currently in use for modern aircraft systems [6, 11, 30, 38] are unsuitable for adaptive flight control systems because they rest on the assumption that the control system is linear (at least locally). The need for completely new V&V techniques is expounded in [10, 9], and some necessary features of a successful V&V procedure are laid out in [18]. Some specific techniques have been proposed for neural network based controllers. For example, the method in [17] relies on bounding neural network outputs using Lipschitz conditions imposed on the chosen set of basis functions, and a second method employs Support Vector Machines (SVM) to determine if a neural network will produce an output that is out of specification [24]. These methods are specific to neural network based adaptive control systems, and it is difficult to envision their use in an industry setting due to their complicated and theoretical nature. In chapter 2 we address this problem by deriving the RLAS. We propose a simple design and verification techniques based on the RLAS that can be used to verify transient properties of adaptive systems. In chapter 3 the RLAS design and verification procedure is applied to two realistic flight control problems.

1.3 Saturation with Multiple Inputs

Another consideration of chief importance in the adaptive control of safety critical systems is that of input saturation. Control of systems with constrained inputs is a theoretically challenging problem and one of immense practical importance. Actuators subject to saturation and bandwidth constraints are ubiquitous in control applications. Actuator constraints can degrade system performance and potentially lead to instability if they are not accounted for in control system design. In particular, adaptive control techniques are especially susceptible to destabilization from saturating actuators since saturation errors can lead to parameter estimation errors,

in turn leading to instability.

In [20, 23, 26, 8, 36, 3], adaptive control approaches for plants in the presence of saturation have been developed. In [20], Karason and Annaswamy introduce a saturation compensation method for direct-adaptive control and show that for a single input plant with output feedback, bounded trajectories can be guaranteed for a range of initial conditions regardless of the stability properties of the open-loop plant. Reference [23] presents a modification of [20] that allows for stable adaptation without hard actuator saturation. In [26], a viable control strategy is proposed without formal proof of stability or boundedness. In [8], the authors review the current state of the art of adaptive control with input constraints. They note that most current algorithms are applicable to indirect-adaptive control, and many rest on the assumption that the plant is open-loop stable. No multi-input saturation compensation strategies are mentioned. An indirect adaptive control strategy is developed in [36] for open-loop stable plants with possible zeros in the RHP. In [3], current saturation compensation methods are used for the problem of reconfigurable flight control.

All of these papers have focused primarily on single input, single output (SISO) systems. To the author's knowledge, there currently exist no formal attempts to demonstrate stability or boundedness for multi-input, multi-output (MIMO), direct-adaptive systems subject to saturation constraints. In fact, it can be argued that susceptibility to saturation errors is a major factor inhibiting the implementation of direct-adaptive control in a wide range of MIMO applications. In chapter 4 we derive a stable adaptive control law for systems with multiple constrained inputs.

1.4 The Reconfiguration Problem

Finally, in chapter 5, we apply the multi-input saturation technique to design a reconfigurable flight controller for a realistic aircraft model with actuator failures and uncertain dynamics. A reconfigurable controller is one that automatically redesigns control laws so as to restore nominal control of a plant in the event of actuator failure or other unforeseen changes in the plant dynamics. Reconfigurable controllers have

the potential to provide a significant benefit in safety in several applications; most notably in aircraft. It is estimated that 14% of all fatal aircraft failures could have been prevented, in principle, by an effective reconfigurable flight control system [14]. Reconfigurable control is crucial to the development of Unmanned Air Vehicles (UAV's) as well, since UAV's are required to follow navigational commands in the presence of uncertain, possibly failure-related, disturbances. Several approaches to reconfigurable control have been proposed for various applications [15, 28, 19], however, this work will focus primarily on the use of adaptive control for reconfiguration.

Most modern aircraft have redundant control effectors, and thus employ so-called control allocation techniques [39]. For such aircraft, it is logical to use the actuator redundancy for the problem of reconfiguration. In other words, if an actuator fails then it might be possible to compensate for its adverse effects by utilizing the remaining healthy controls. Control allocation algorithms such as Pseudo-Inverse [39], Quadratic Programming [5], Linear Programming [13], Direct Allocation [12], and others have been applied to the problem of reconfiguration with varying degrees of success. Specifically, Durham's Direct Allocation has received much attention recently, and has been shown to be among the most promising allocation algorithms [12, 29].

To be useful for reconfiguration, all of the above allocation methods require an online estimate of the aircraft dynamics after failure. The speed of convergence of such online estimators depends on excitation of the external inputs, which can be somewhat alleviated by using multiple models as demonstrated by Boskovic and Mehra [4]. In light of these potential difficulties, another direction of research has focused on reconfiguration with fixed allocation [40, 2, 21, 7, 37] where direct-adaptation can be applied straightforwardly in the realm of virtual-inputs. In [40] a reconfiguration retrofit module is developed for transport aircraft, with a direct-adaptive input error approach. In [2] several adaptation methods are examined, and it is concluded that a direct-adaptive input error formulation is most appropriate for the problem of reconfiguration. Similar techniques are used in [21] with a cascading adaptive formulation, and in [7] with an adaptive neural network. In [37], Tao et. al. consider

direct-adaptation for reduced order, single input systems representative of aircraft dynamics. In all of these cases, the controller was assumed to operate with fixed control allocation. This is an inherent shortcoming because it fails to utilize the versatility of an over-actuated aircraft. Specifically, it requires that independent control surfaces be restricted to move in constant proportion to one another, thereby limiting the moments attainable by the control system. The controller derived in chapter 5 attempts to combine the benefits of control allocation and direct adaptive control while avoiding the drawbacks of either.

Chapter 2

Verifiable Transient Properties

2.1 Introduction

In this chapter, we introduce a tool based on Lyapunov theory, asymptotic analysis, and linear systems theory for analyzing the transient behavior and disturbance rejection properties of adaptive systems. At the same time, the tool provides practical guidelines for tuning adaptive controllers to satisfy predetermined performance criteria. The focus of this chapter is limited to the simplest embodiment of a direct adaptive controller: Model Reference Adaptive Control (MRAC) using state feedback for a single input plant. In section 2.2, a general plant model is introduced and its scope is discussed. In section 2.3 a simple direct adaptive control architecture is developed for the model. In section 2.4, the Reduced Linear Asymptotic System (RLAS) is derived and it's relevance to the problem is proven. Section 2.5 describes a design procedure using the RLAS to produce adaptive designs with specified transient properties. In section 2.6 we describe a procedure for using the RLAS to verify the transient properties of an adaptive control design. Section 2.7 aims to characterize the covergence rate from the nonlinear system to the RLAS. An approach to the inherently nonlinear analysis is proposed in this section. Finally, a summary is given section 2.8

2.2 Model Development

The problem under consideration is the control of an uncertain, states accessible, nonlinear plant of the form

$$\dot{X} = f_p(X, U)$$

where $X \in \Re^n$ and $U \in \Re$. For the purposes of control, the nonlinear plant is approximated by a schedule of Linear Time-Invariant (LTI) systems of the form

$$\dot{x} = A_p x + b_p \delta_{ad} + d_p \tag{2.1}$$

where $x = X - X_0$, and $\delta_{ad} = U - U_0$, and where $A_p \in \Re^{n \times n}$, $b_p \in \Re^n$, and $d_p \in \Re^n$ are unknown. X_0 is a desired equilibrium state and U_0 is an unknown constant "trim" input that maintains the plant at X_0 in the absence of the disturbance d_p. Specifically, X_0 and U_0 satisfy the relation $b_p U_0 = -A_p X_0$. It is desired that the plant follow a known reference model, which itself is nonlinear and of the form

$$\dot{X}_m = f_m(X_m, U_m)$$

where $X_m \in \Re^n$, and $U_m \in \Re$ is a bounded input from a pilot or a guidance/navigation system. Moreover, the reference model is also expressed as a schedule of known LTI systems with a known interpolation algorithm. Each LTI reference model can be written as:

$$\dot{x}_m = A_m x_m + b_m \delta_c \tag{2.2}$$

where $x = X - X_0$, and $\delta_{ad} = U - U_0$. It is assumed that $A_m \in \Re^n$ is Hurwitz, and X_0 is the same equilibrium state used in Eq. (2.1), and U_{m_0} is the necessary trim input for the reference model, so that $b_m U_{m_0} = -A_m X_0$.

In this work, each LTI plant-reference model pair (Eqs. (2.1) and (2.2)) will be treated separately, as is common in flight dynamics. It is assumed that the above scheduled representation of a nonlinear system is adequate for the problem at hand and questions pertaining to inaccuracies of this representation will not be consid-

ered in this chapter. The representation described above is typical of flight vehicle dynamics. Note that equation (2.1) may include physical dynamics as well as feedback dynamics imposed by the presence of a nominal controller, and the state x may include controller states, such as integrators, as well as other physical parameters.

2.3 Direct Adaptive Controller

We would like to design a control input $\delta_{ad}(x, x_m, \delta_c)$ such that

$$\lim_{t\to\infty}(x - x_m) = 0. \tag{2.3}$$

Let the input, δ_{ad}, be given by the control law

$$\delta_{ad} = \theta^T \omega. \tag{2.4}$$

$$\text{where} \quad [\ x^T \quad \delta_c \quad 1\ ]^T \quad \text{and} \quad [\ \theta_x^T \quad \theta_\delta \quad \theta_d\ ]^T, \tag{2.5}$$

and $\theta_x \in \Re^n$, $\theta_\delta \in \Re$, and $\theta_d \in \Re$ are control gains. The control gains are adjusted according to the adaptation law

$$\dot{\theta} = -\Gamma \omega b_m^T P e, \tag{2.6}$$

where $e = x - x_m$ is the system tracking error, P is the unique symmetric positive definite solution of the algebraic Lyapunov equation $A_m^T P + P A_m = -Q$, with $Q > 0$. Also, in (2.6), $\Gamma > 0$ is a positive definite symmetric matrix of adaptation rates. Assuming that there exist ideal gains θ_x^*, $\theta_\delta^* > 0$, and θ_d^* such that

$$b_p \theta_x^{*T} = A_m - A_p, \quad b_p \theta_\delta^* = b_m, \text{ and } \quad b_p \theta_d^* = d, \tag{2.7}$$

the controller in (2.4) with the control law in (2.6) can be shown to achieve tracking as specified in (2.3). Equations (2.7) are known as the model matching conditions.

The control gains can then be redefined in terms of the ideal gains and gain errors as

$$\tilde{\theta}_x = \theta_x - \theta_x^*, \quad \tilde{\theta}_\delta = \theta_\delta - \theta_\delta^*, \text{ and } \quad \tilde{\theta}_d = \theta_d = \theta_d^*. \tag{2.8}$$

Substituting equations (2.1), (2.2), (2.4), (2.6), (2.7), and (2.8), and recalling that $e = x - x_m$ gives

$$\begin{bmatrix} \dot{e} \\ \dot{\tilde{\theta}} \end{bmatrix} = \begin{bmatrix} A_m & \lambda_\delta b_m \omega^T \\ -\Gamma \omega b_m^T P & 0 \end{bmatrix} \begin{bmatrix} e \\ \tilde{\theta} \end{bmatrix}, \tag{2.9}$$

where $\lambda_\delta = 1/\theta_\delta^*$, and $\tilde{\theta} = [\ \tilde{\theta}_x^T \quad \tilde{\theta}_\delta \quad \tilde{\theta}_d\ ]^T$. Equation (2.9) represents the error dynamics of the closed loop adaptive system. Notice that the error dynamics are nonlinear and time varying due to the presence of the linear regressor vector ω. The problem considered in this chapter is how to design adaptation gains Γ and Q in (2.9) to produce an adaptive response for a given specification, and, once designed, how to verify that the response is indeed within the given specification.

2.4 RLAS: An Adaptive Control Design Tool

The tools are here presented in two theorems which are then proven. The first theorem states the well known properties of MRAC systems based on Lyapunov analysis. The second theorem introduces the Linear Asymptotic System (LAS), which emerges from an asymptotic analysis of (2.9). The LAS is then simplified to give the Reduced Linear Asymptotic System (RLAS).

Theorem 2.1 *The error dynamics in equation (2.9) have the following properties:*

i) the plant state x is bounded,

ii) the controller gains θ are bounded,

iii) $\lim_{t\to\infty} e = 0$.

Proof

Consider the Lyapunov function candidate

$$V = e^T P e + \tilde{\theta}^T \lambda_\delta \Gamma^{-1} \tilde{\theta}. \tag{2.10}$$

Taking time derivatives along the system trajectories gives $\dot{V} = -e^T Q e \leq 0$. This implies that V is bounded, and hence e and $\tilde{\theta}$ are bounded. Since A_m is stable and δ_c is bounded, x_m is bounded. This, in turn, implies that x and θ are bounded, and *i)* and *ii)* are proven. Now, x bounded and δ_c bounded imply ω is bounded; and A_m stable, e bounded, and $\tilde{\theta}$ bounded imply that $\dot{e}$ is bounded. This implies that $\ddot{V}$ is bounded. Therefore, by Barabalat's lemma, $\lim_{t\to\infty} \dot{V} = 0$, which directly implies *iii)*.

∇

Definition 2.1 *A dynamics, $\dot{z}_1 = f(z_1)$, is said to converge to another dynamics, $\dot{z}_2 = g(z_2)$, if given an ϵ, there exists T such that for each initial condition $z_1(t_0)$ and $z_2(t_0)$,*

$$\|z_1(t) - z_2(t)\| \leq \epsilon \quad \forall t \geq t_0 + T.$$

Theorem 2.2 *For a constant input, δ_c, the error dynamics in equation (2.9) converge to the dynamics*

$$\begin{bmatrix} \dot{e}_a \\ \dot{\tilde{\theta}}_a \end{bmatrix} = \begin{bmatrix} A_m + \lambda_\delta b_m \theta_{x_c}^T & \lambda_\delta b_m \omega_{m_c}^T \\ -\Gamma \omega_{m_c} b_m^T P & 0 \end{bmatrix} \begin{bmatrix} e_a \\ \tilde{\theta}_a \end{bmatrix}, \tag{2.11}$$

where $\omega_{m_c} \in \Re^{n+2}$ is a known constant, and $\lambda_\delta \in \Re$ and $\theta_{x_c} \in \Re^n$ are unknown bounded constants.

Proof

The linear regressor, ω, can be written

$$\omega = \omega_e + \omega_m,$$

$$\text{where} \quad \omega_e = \begin{bmatrix} e^T & 0 & 0 \end{bmatrix}^T, \text{ and } \quad \omega_m = \begin{bmatrix} x_m^T & \delta_c & 1 \end{bmatrix}^T.$$

With δ_c constant and A_m stable, ω_m converges exponentially to a constant ω_{mc}, where

$$\omega_{mc} = [\ x_{m_c}^T \quad \delta_c \quad 1\ ]^T, \text{ and } \quad x_{mc} = -A_m^{-1} b_m \delta_c.$$

Therefore the error dynamics in (2.9) converge exponentially to a new error dynamics, which can be expressed as

$$\begin{bmatrix} \dot{e}_t \\ \dot{\tilde{\theta}}_t \end{bmatrix} = \begin{bmatrix} A_m & \lambda_\delta b_m \omega_{m_c}^T \\ -\Gamma \omega_{mc} b_m^T P & 0 \end{bmatrix} \begin{bmatrix} e_t \\ \tilde{\theta}_t \end{bmatrix} + \begin{bmatrix} \lambda_\delta b_m \omega_{e_t}^T \tilde{\theta}_t \\ -\Gamma \omega_{et} b_m^T P e_t \end{bmatrix}, \tag{2.12}$$

where $\omega_{et} = [\ e_t^T \quad 0 \quad 0\ ]^T$. Notice that (2.12) is time-invariant and nonlinear.

We now show that for a constant input, δ_c, the parameter error, $\tilde{\theta}$, converges to an unknown constant vector $\theta_c = [\ \theta_{x_c}^T \quad \theta_{\delta_c} \quad \theta_{d_c}\ ]^T$. To prove this, recall the Lyapunov function (2.10). Since $\dot{V} \leq 0$, by La Salle's Invariance Principle [22] the state $e, \tilde{\theta}$ converges to its largest invariant set. This implies that $lim_{t\to\infty} \dot{e} = 0$ and $lim_{t\to\infty} \dot{\tilde{\theta}} = 0$. From theorem 2.1 and from (2.9) this implies that $lim_{t\to\infty} \omega^T \tilde{\theta} = 0$. Therefore

$$lim_{t\to\infty} \tilde{\theta} = \theta_{x_c},$$

where $\omega_{m_c}^T \theta_{x_c} = 0$.

Using this fact and Theorem 2.1, the dynamics in (2.12) can be expanded in a Taylor series about the equilibrium point $e_t = 0$ and $\tilde{\theta}_t = \theta_c$ to give

$$\begin{bmatrix} \dot{e}_a \\ \dot{\tilde{\theta}}_a \end{bmatrix} = \begin{bmatrix} A_m + \lambda_\delta b_m \theta_{x_c}^T & \lambda_\delta b_m \omega_{m_c}^T \\ -\Gamma \omega_{mc} b_m^T P & 0 \end{bmatrix} \begin{bmatrix} e_a \\ \tilde{\theta}_a \end{bmatrix} + \begin{bmatrix} f\left(e_a, \tilde{\theta}_a\right) \\ g\left(e_a, \tilde{\theta}_a\right) \end{bmatrix}, \tag{2.13}$$

where f and g contain only second order terms. Using Definition 2.1, Theorem 2.2 follows directly.

∇

The properties of chief interest for V&V are the asymptotic state error dynamics, e_a, and the input dynamics, δ_{ad}. Define the asymptotic input error dynamics to be

$$\tilde{\delta}_a = \omega_{m_c}^T \tilde{\theta}_a. \tag{2.14}$$

Substituting (2.14) into (2.11) and simplifying gives

$$\begin{bmatrix} \dot{e}_a \\ \dot{\tilde{\delta}}_a \end{bmatrix} = \begin{bmatrix} A_m + \lambda_\delta b_m \theta_{x_c}^T & \lambda_\delta b_m \\ -\gamma b_m^T P & 0 \end{bmatrix} \begin{bmatrix} e_a \\ \tilde{\delta}_a \end{bmatrix}, \tag{2.15}$$

where γ is defined to be the known scalar $\omega_{m_c}^T \Gamma \omega_{m_c}$. Equation (2.15) is the Reduced Linear Asymptotic Systems (RLAS). Notice that the LAS (2.11) has $2n+2$ eigenvalues, $n+1$ of which are stable and the remaining $n+1$ are identically zero. The RLAS has $n+1$ stable eigenvalues, which are equal to the $n+1$ stable eigenvalues of the LAS. The RLAS is a simple, linear, compact approximation to the dynamics of the closed loop adaptive system. It is the main tool used in this chapter and the next to predict the oscillatory behavior of adaptive systems for design or verification purposes.

2.5 RLAS Design Procedure

The optimal selection of Γ and Q in (2.9) for a given set of performance metrics is the eventual goal of this research. The RLAS is useful toward this end because Γ and Q can be designed for the RLAS using linear design techniques to meet the given performance metrics. The same Γ and Q can then be applied to the adaptive system, which is proven to converge to the RLAS, and therefore, will satisfy the performance metrics as well, after the transient delay. In this section we take a first step toward this goal and find Γ and Q by a combination of analysis and numerical simulations.

In order to find the optimal Γ and Q, the unknown quantities λ_δ and θ_{x_c} in (2.15) must be estimated. In this study, λ_δ, the control effectiveness uncertainty, was chosen as an example of an extraordinary failure, though in practice expected bounds

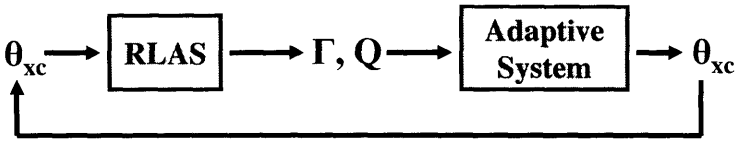

Figure 2-1: The figure illustrates the iterative procedure used to determine the values of Γ, Q, and θ_{x_c}.

on λ_δ would have to be determined based on the specifics of the plant and its range of operation. The asymptotic gain error, θ_{xc}, was estimated in an iterative process in the following way. The unknown value θ_{xc} was set to zero in the RLAS (2.15) and suitable values of Γ and Q were determined using the root locus method. The trajectory of the adaptive dynamics (2.9) was then found through numerical simulation using these values of Γ and Q, and a new value of θ_{xc} was determined. This process was repeated until a value of θ_{xc} was converged upon. The iterative procedure is illustrated in figure 2-1. In practice, only one or two iterations were required since it was found that the RLAS dynamics were typically not sensitive to variations in θ_{xc}. This observation can be verified with a root locus of the RLAS with respect to each of the elements of θ_{xc}. In the future it would be interesting to investigate methods for analytically estimating θ_{xc}, or bounding its effect on the RLAS, to avoid this iterative procedure.

We now discuss how Γ and Q are determined for a given value of θ_{xc}. It is known in a qualitative sense that increasing Γ and Q will cause more vigorous oscillation and less overshoot in an adaptive system. The proposed RLAS design approach allows these intuitions to be formalized. In the RLAS the pilot/navigation system input, δ_c, and the adaptive gain Γ appear as a single scalar, γ. A root locus of (2.15) with respect to γ can be used to verify the intuition that increasing Γ increases response frequency. Likewise, the RLAS gives the additional insight that the response frequency is roughly proportional to the square of the input signal δ_c. Thus if one wishes to limit the frequency of the adaptive response, one must have some control, or at least some known bounds, on the input signal. The effects of the elements of the vector $b_m^T P$ can be determined similarly, noting that increasing these elements leads to a more oscillatory response. Therefore, γ and $b_m^T P$ can be designed for the RLAS

using the common arsenal of linear design techniques, such as the root locus method, Bode plots, or Nyquist plots. These can then be used to back calculate Γ and Q straightforwardly, taking care that both P and Q in the linear Lyapunov equation are positive definite. For the studies in this work, Γ and Q were determined using the root-locus method to obtain suitable eigenvalues for the RLAS. In particular, these values were chosen so that the oscillatory mode of the RLAS corresponded to a given design specification, while all 1st order modes were sufficiently fast not to inhibit response time.

2.6 RLAS Verification Procedure

The RLAS can further be used to verify the adaptive design by comparing its trajectory to that of the adaptive system. For this procedure, we explicitly simulate the response of the RLAS and the adaptive system under some known failure (or uncertainty) to ascertain how close their responses are and how quickly they converge. The RLAS was formulated as previously (2.15) using the same values of λ_δ and θ_{xc}. To give a meaningful comparison with the trajectory of the adaptive system, the RLAS trajectory must be added to the reference model trajectory to obtain a corresponding linear "state" trajectory. For this purpose, an appropriate set of initial conditions $e_a(t_0)$ and $\tilde{\delta}_a(t_0)$ for the RLAS must be calculated from the corresponding conditions of the adaptive system at t_0. The initial error, $e_a(t_0)$ is easily found from the initial states of the adaptive system and reference model as $e_a(t_0) = x(t_0) - x_m(t_0)$, while the initial input error $\tilde{\delta}_a(t_0)$ is found from $\tilde{\delta}_a(t_0) = \omega_{mc}(\theta(t_0) - \theta^*)$. Comparison of the trajectories can then be used to infer whether the adaptive system satisfies the design criteria. In the following chapter we will apply such a design/verification methodology to design an adaptive controller with suitable transient properties for a linear model of the aircraft short period mode and for a full nonlinear 6-DOF aircraft model.

2.7 Nonlinear Transients

Theorem 2.2 ensures that the dynamics converge to an RLAS, but one crucial piece of information that this theorem does not provide is the rate at which convergence is achieved. Unfortunately, the question of convergence rates for nonlinear systems, such as the adaptive error dynamics in (2.9), is a difficult one, and in general there is no method of determining such a rate. It would be valuable to be able to characterize the convergence rate as bounded by some exponential curve (exponential convergence). In this section we set forth a simple geometric requirement for exponential convergence, however a means of proving that the requirement is verified for the dynamics in (2.9) is out of reach at present.

We consider the simplest case of the dynamics in (2.9) which still retains the necessary qualities of the system. In particular, let $e \in \Re$, $\theta \in \Re^2$, $b_m = 1$, and $A_p = a_p \in \Re$ and $\lambda_\delta = \lambda \in \Re$ are both uncertain. Also, we let $\Gamma = I_2$ and we make the assumption that $\omega_m(t) = \omega_{m_c}\ \forall t$. For this case, the dynamics in (2.9) can be written

$$\begin{bmatrix} \dot{e} \\ \dot{\tilde{\theta}} \end{bmatrix} = \begin{bmatrix} a_m & \lambda\omega^T \\ -\omega & 0 \end{bmatrix} \begin{bmatrix} e \\ \tilde{\theta} \end{bmatrix}. \tag{2.16}$$

Breaking the system into linear and nonlinear parts and using the relations $\omega = \omega_e + \omega_{m_c}$ and $\tilde{\theta} = \tilde{\theta_a} + \theta_c$ we can write the dynamics in (2.17) as

$$\begin{bmatrix} \dot{e} \\ \dot{\tilde{\theta}} \end{bmatrix} = \begin{bmatrix} a_m + \theta_{x_c} & \lambda\omega_{m_c}^T \\ -\omega_{m_c} & 0 \end{bmatrix} \begin{bmatrix} e \\ \tilde{\theta} \end{bmatrix} + \begin{bmatrix} \lambda\omega_e^T\tilde{\theta_a} \\ \omega_e e \end{bmatrix}. \tag{2.17}$$

Close to the equilibrium, the linear terms dominate and exponential convergence is ensured. Therefore we must examine the nonlinear terms away from the equilibrium. The term $\omega_e e$ is quadratic and, therefore, contributes to faster than exponential convergence away from the origin. The term $\lambda\omega_e^T\tilde{\theta_a}$ is not necessarily large away from the origin since it is possible that $\lambda\omega_e^T\tilde{\theta_a} = 0$ when $\omega_e \neq 0$ and $\tilde{\theta_a} \neq 0$ if ω_e and $\tilde{\theta_a}$ are perpendicular. Thus the convergence rate of the adaptive system depends upon the relative orientation of ω_e and $\tilde{\theta_a}$. Also, recall that $\omega_e = [\ e\ \ 0\ ]^T$, therefore $\lambda\omega_e^T\tilde{\theta_a} = 0$

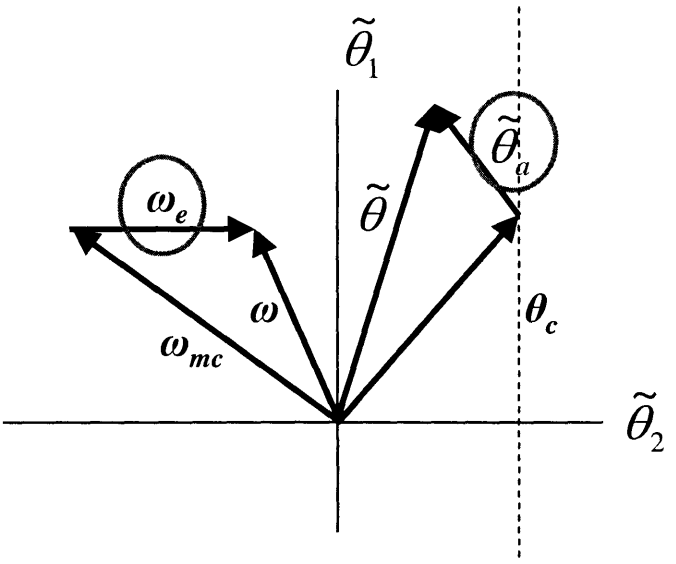

Figure 2-2: The figure shows the vector quantities that determine the convergence rates of the bilinear term. For exponential convergence, $\tilde{\theta_a}$ must not become perpendicular to ω_e.

only when $\tilde{\theta_a} = [\ 0 \quad \tilde{\theta}_{\delta_a}\ ]^T$. So the requirement for exponential convergence becomes that $\tilde{\theta_a} \neq 0\ \forall t$. This is depicted graphically in figure 2-2.

We have shown in simulation that this requirement can be satisfied for sufficiently small initial conditions. However, even when this requirement is not met, the simulation results in the next chapter show that in practice the convergence rates of the nonlinear terms are indeed faster than the linear dynamics and play an insignificant role in the over-all transient characteristics of the adaptive system.

2.8 Summary

In this chapter we introduced a new tool for designing and verifying the oscillatory properties of adaptive systems. The RLAS was formulated to provide a compact linear approximation to nonlinear adaptive systems. General design and verification techniques using the RLAS were then described.

Chapter 3

Designing to Transient Specifications

3.1 Introduction

The tools developed in the previous chapter are here applied to two examples. First, the usefulness of the RLAS approach is demonstrated using linear uncertain short period aircraft dynamics with a state feedback nominal controller. The adaptive controller is applied to the closed loop nominal system in an architecture that will be referred to as adaptive augmentation. The design and verification capabilities of the RLAS are then demonstrated in a simulation environment. Secondly, a more realistic application is considered, in which the design and verification techniques are applied to a full-nonlinear 6-DoF aircraft simulation. An LQ nominal controller with integral action is designed to control the short period motion of the aircraft using the uncertain, linear short period approximation. The adaptive loop is closed around the closed loop nominal system to produce the adaptive augmented control architecture. Simulation results are presented to verify the design and demonstrate the usefulness of the RLAS.

In section 3.2 the linear short period model is introduced and the nominal LQ state feedback controller is designed for the model. Section 3.3 details the development of the adaptive augmentation and derives the RLAS for the closed loop short

period system. In section 3.4 the design and verification procedures descried in the previous chapter are applied to the short period model and results are presented from numerical simulation. The nonlinear aircraft model and nominal LQ controller with integral action are introduced in section 3.5. Section 3.6 develops the adaptive augmented controller and derives the RLAS for the system. In section 3.7 the design and verification procedures described in the previous chapter are applied to the nonlinear model and numerical simulation results are presented. Conclusions and directions for future research are given in section 3.8.

3.2 Short Period Model and Nominal Controller

From [35], short period dynamics of a fixed-wing aircraft with zero bank angle can be expressed as

$$\begin{bmatrix} \dot{\alpha} \\ \dot{q} \end{bmatrix} \begin{bmatrix} -L_\alpha & -L_q \\ \lambda_\alpha M_\alpha & \lambda_q M_q \end{bmatrix} \begin{bmatrix} \alpha \\ q \end{bmatrix} + \lambda_\delta \begin{bmatrix} 0 \\ M_\delta \end{bmatrix} (\delta + d_{trm}) . \tag{3.1}$$

In 3.1, α is the aircraft angle of attack (AOA) and q is the body pitch rate. The scalars $\lambda_\delta > 0$, λ_α, and λ_q represent uncertainties in the parameter values, and d_{trm} denotes an unknown trim input component. In addition, it is assumed that the aircraft state vector, $x = [\ \alpha \quad q\ ]^T$, is available on-line for control purposes. The rest of the parameters represent the so-called aircraft stability and control derivatives. The values of the stability and control derivatives used in this example are

$$L_\alpha = 0.6582, \quad L_q = -0.9705, \quad M_\alpha = -3.3105, \quad M_q = -1.4741, \text{ and } \quad M_\delta = -3.6764.$$

They were found from a numerical linearization of a nonlinear aircraft model (see section 3.5 for details). The dynamics in (3.1) can be expressed compactly as

$$\dot{x} = Ax + \lambda_\delta b (\delta + d_{trm}) . \tag{3.2}$$

Likewise, let the dynmaics without uncertainty (i.e. (3.1) where $\lambda_\alpha = \lambda_q = \lambda_\delta = 1$, and $d_{trm} = 0$), be denoted

$$\dot{x}_{sp} = A_{sp}x_{sp} + b_{sp}\delta. \tag{3.3}$$

A nominal controller is designed assuming no uncertainty as in (3.3) and applied to the uncertain dynamics in (3.1). The Linear Quadratic (LQ) optimal control design technique [25] is straightforwardly applied to the dynamics in (3.3). A state-feedback controller architecture is used for the nominal controller so that

$$\delta_{nom} = k_x^T x + k_\delta \delta_c, \tag{3.4}$$

where $k_x = [\ k_\alpha \quad k_q\ ]^T$. The feedback gain, k_x, is found by minimizing the cost function

$$J = \frac{1}{2}\int_0^\infty x^T \left(Q_J + k_x^T R_J k_x\right) x dt, \tag{3.5}$$

subject to the dynamics in (3.3). A suitable closed loop response is found with $Q_J = diag([\ 2 \quad 1\ ])$ and $R_J = 1$ to give the feedback gains $k_x = [\ -0.2816 \quad -0.7434\ ]^T$. The feed forward gain, k_δ, is designed to produce angle of attack following so that $k_\delta = 1/g_\alpha$, where $[\ g_\alpha \quad g_q\ ]^T = -[A_{sp} + b_{sp}k_x]^{-1}b_{sp}$ is the steady state gain of (3.3) with the feedback component k_x. Then the closed loop dynamics of (3.3) with control law (3.4) can be written

$$\dot{x}_m = A_m x_m + b_m \delta_c, \tag{3.6}$$

where $A_m = (A_{sp} + b_{sp}k_x)$ and $b_m = b_{sp}k_\delta$. Defining the input to the actual dynamics (3.2) to be $\delta = \delta_{nom} + \delta_{ad}$, the actual closed loop dynamics becomes

$$\dot{x} = (A + \lambda_\delta b k_x)\, x + \lambda_\delta b\, (\delta ad + d_{trm})\,. \tag{3.7}$$

3.3 Adaptive Augmentation and RLAS

Assume that we desire for the uncertain closed loop system (3.7) to follow the closed loop system without uncertainty (3.6). We can use (3.6) as a reference model for

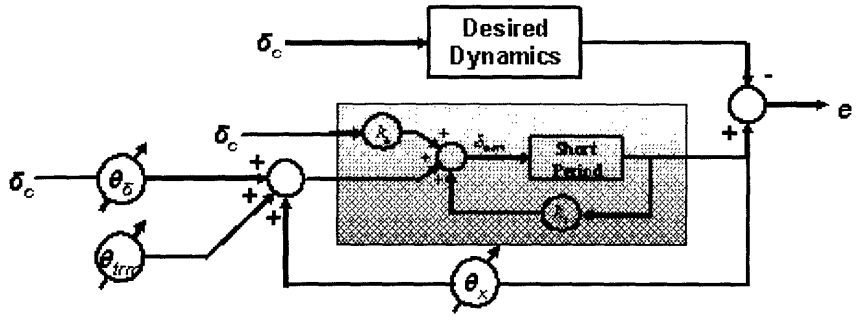

Figure 3-1: A block diagram of the augmented adaptive system for the short period dynamics with multiple parameter uncertainties is shown.

an adaptive controller designed as in (2.4) and (2.6). The combined nominal and adaptive architecture is referred to as an adaptive augmented controller. Using (2.4) and (2.6), and (3.1) and (3.7), the error dynamics can be represented as

$$\begin{bmatrix} \dot{e} \\ \dot{\tilde{\theta}} \end{bmatrix} = \begin{bmatrix} A_m & \lambda_\delta b\omega^T \\ -\Gamma\omega b^T P & 0 \end{bmatrix} \begin{bmatrix} e \\ \tilde{\theta} \end{bmatrix}, \tag{3.8}$$

where $\tilde{\theta} = \theta - \theta^*$, and $\theta^* = [\ \theta_\alpha^* \quad \theta_q^* \quad \theta_\delta^* \quad \theta_{trm}^*\ ]^T$, and where $\theta_\alpha^* = \frac{M_\alpha(1-\lambda_\alpha)+k_\alpha M_\delta(1-\lambda_\delta)}{\lambda_\delta M_\delta}$, $\theta_q^* = \frac{M_q(1-\lambda_q)+k_q M_\delta(1-\lambda_\delta)}{\lambda_\delta M_\delta}$, $\theta_\delta^* = \frac{k_\delta(1-\lambda_\delta)}{\lambda_\delta}$, and $\theta_{trm}^* = -d_{trm}$. A block diagram of the adaptive augmented systems is shown in Fig. 3-1. The RLAS can be seen directly from (2.15) and (3.8) to be

$$\begin{bmatrix} \dot{e}_a \\ \dot{\tilde{\delta}}_a \end{bmatrix} = \begin{bmatrix} A_m + \lambda_\delta b\theta_{x_c}^T & \lambda_\delta b \\ -\gamma b^T P & 0 \end{bmatrix} \begin{bmatrix} e_a \\ \tilde{\delta}_a \end{bmatrix}, \tag{3.9}$$

where $\gamma = \omega_{mc}^T \Gamma \omega_{mc}$, and $\omega_{mc} = [\ -(A_m^{-1} b_m \delta_c)^T \quad \delta_c \quad 1\ ]^T$.

3.4 Design and Verification Procedure

The design procedure described in section 2.5 was carried out using the error dynamics in (3.8) and the RLAS in (3.9). The RLAS was tuned to produce a response within the military specification for the short period mode frequency and damping ratio

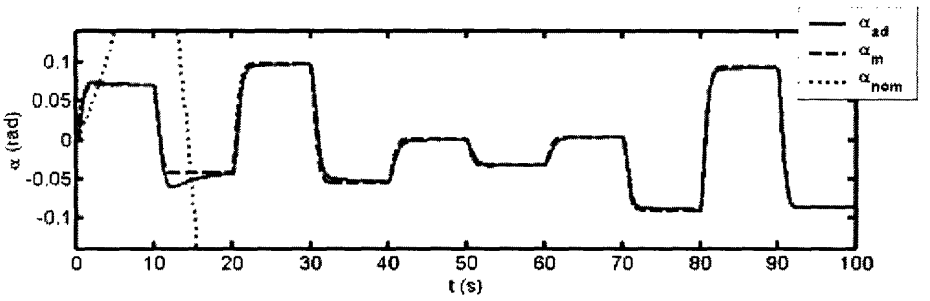

Figure 3-2: The α trajectory of the adaptive augmented system is shown with uncertainties $\lambda_\alpha = -1$, $\lambda_q = 0.9$, $\lambda_\delta = 0.7$, and $d_{trm} = 0.1$. The RLAS was used to design a suitable adaptive response to a random amplitude square-wave input. The trajectories of the reference model and the nominal system are shown for comparison. Note that the nominal system is unstable.

(MIL-F-8785C) [1]. This specification requires that, for Category A flight phase (requiring rapid maneuvering) and Level 1 flying qualities (qualities adequate for the flight phase) the allowable ranges for damping ratio, ζ, and natural frequency, ω_n, are

$$0.35 \leq \zeta \leq 1.35 \quad \text{and} \quad 0.653 rad/s \leq \omega_n \leq 8.39 rad/s. \tag{3.10}$$

The design procedure resulted in $\Gamma = diag([\ 100 \quad 100 \quad 100 \quad 1\ ])$ and $Q = diag([\ 2 \quad 1\ ])$ which give the damping ratio $\zeta = 0.518$, the natural frequency $\omega_n = 4.95 rad/s$, and the 1st order time constant $t = 3.57s$.

A severe failure was simulated by setting, the uncertainties to be $\lambda_\alpha = -1$, $\lambda_q = 0.9$, $\lambda_\delta = 0.7$, and $d_{trm} = .01$. In figs. 3-2 and 3-3 the responses to a random amplitude square wave input of the adaptive system and the nominal system are shown for this failure. It can be seen that the nominal system becomes unstable whereas the adaptive system is stable and tracks the reference model asymptotically. The response of the adaptive system clearly provides suitable flying qualities using the RLAS design methodology.

The verification of the design was carried out according to the procedure in section 2.6. In figs. 3-4 and 3-5, and in figs. 3-6 and 3-7, the trajectories of α and q are shown for $t = 0s$ to $t = 5s$ and for $t = 80s$ to $t = 85s$ respectively, for both the adaptive

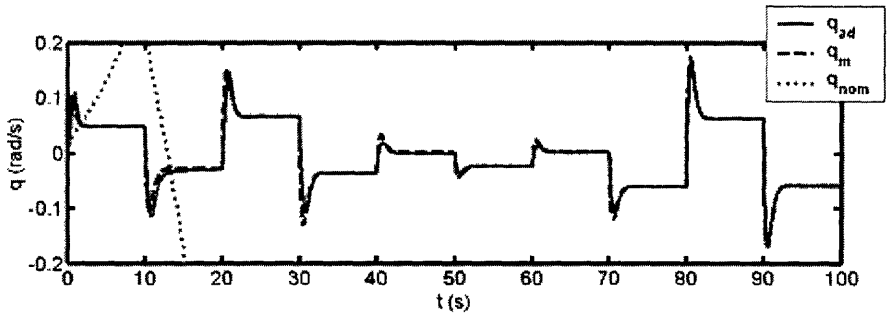

Figure 3-3: The q trajectory of the adaptive augmented system is shown with uncertainties $\lambda_\alpha = -1$, $\lambda_q = 0.9$, $\lambda_\delta = 0.7$, and $d_{trm} = 0.1$. The RLAS was used to design a suitable adaptive response to a random amplitude square-wave input. The trajectories of the reference model and the nominal system are shown for comparison. Note that the nominal system is unstable.

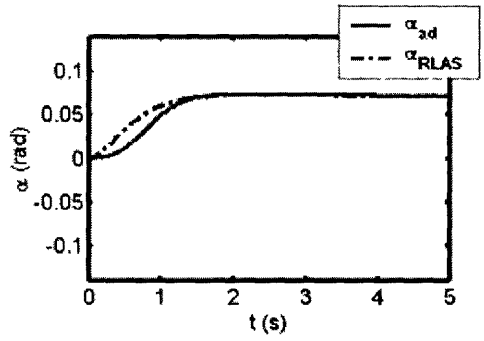

Figure 3-4: Close-ups of the α trajectory from figs. 3-2 is shown here from $t = 0s$ to $t = 5s$. Although the nonlinear system is still in a transient regime, its oscillatory properties are well approximated by the RLAS.

system and the RLAS for the failure described previously. These figures show that the adaptive system converges to the RLAS and hence meets the specification (3.10). Even during inital transients (figs. 3-4 and 3-5), the oscillatory characteristics of the adaptive system are well approximated by the RLAS.

3.5 Nonlinear Model and Nominal Controller

A nonlinear 6-DoF simulation of a large transport aircraft was implemented according to accepted aircraft simulation practices [35]. The aircraft was trimmed with

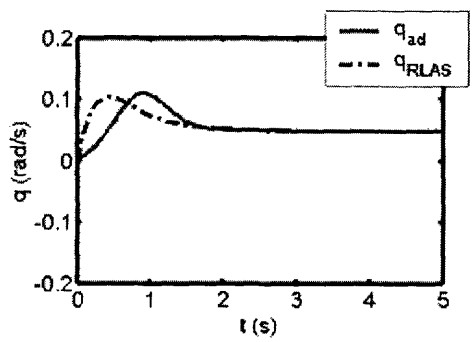

Figure 3-5: Close-ups of the q trajectory from figs. 3-3 is shown here from $t = 0s$ to $t = 5s$. Although the nonlinear system is still in a transient regime, its oscillatory properties are well approximated by the RLAS.

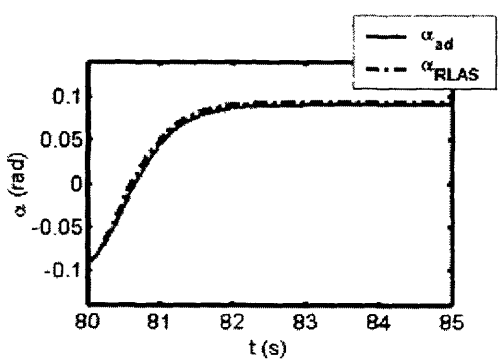

Figure 3-6: Close-ups of the α trajectory from figs. 3-2 is shown here from $t = 80s$ to $t = 85s$. The nonlinear adaptive system tracks the RLAS closely. The RLAS was designed to have one oscillatory mode with $\zeta \approx 0.5$ and $\omega_n \approx 5$ and one first order mode with $\tau \approx 3.6s$ for a response well within military flying qualities specifications.

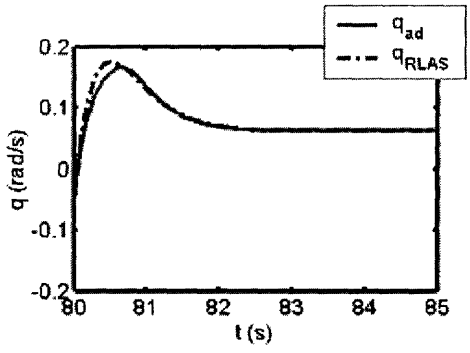

Figure 3-7: Close-ups of the q trajectory from figs. 3-3 is shown here from $t = 80s$ to $t = 85s$. The nonlinear adaptive system tracks the RLAS closely. The RLAS was designed to have one oscillatory mode with $\zeta \approx 0.5$ and $\omega_n \approx 5$ and one first order mode with $\tau \approx 3.6s$ for a response well within military flying qualities specifications.

wings level to ensure that the longitudinal and lateral dynamics were decoupled. The controllers (both the LQ nominal controller and the outer loop adaptive controller) were designed using the short period approximation as a plant model to represent the nonlinear aircraft dynamics. Care was taken to ensure that the short period approximation was valid over the trajectory of interest. The nonlinear aircraft was linearized to produce the longitudinal dynamics. Then the short period approximation was used to derive the second order short period model of (3.3) from the fourth order longitudinal model. The short period dynamics in (3.3) serve as the plant model for the LQ nominal controller and the adaptive controller to be used with the full nonlinear aircraft.

The LQ control design technique [25] is straightforwardly applied using a proportional-integral controller architecture to give zero steady state error to a step input command. The uncertain dynamics in (3.1) are expanded to include an integrator to give

$$\begin{bmatrix} \dot{\alpha} \\ \dot{q} \\ \dot{e}_I \end{bmatrix} \begin{bmatrix} -L_\alpha & -L_q & 0 \\ \lambda_\alpha M_\alpha & \lambda_q M_q & 0 \\ 1 & 0 & 0 \end{bmatrix} \begin{bmatrix} \alpha \\ q \\ e_I \end{bmatrix} + \lambda_\delta \begin{bmatrix} 0 \\ M_\delta \\ 0 \end{bmatrix} (\delta + d_{trm}) + \begin{bmatrix} 0 \\ 0 \\ -1 \end{bmatrix} \delta_c, \quad (3.11)$$

where e_I is the state of an AOA integrator and $\delta = k_x^T + \delta_{ad}$. Equation (3.11) can be written in the compact form $\dot{x} = Ax + \lambda_\delta b\,(\delta + d_{trm}) + b_m\delta_c$, and without uncertainty the dynamics are denoted

$$\begin{bmatrix} \dot{\alpha}_m \\ \dot{q}_m \\ \dot{e}_{I_m} \end{bmatrix} \begin{bmatrix} -L_\alpha & -L_q & 0 \\ M_\alpha + M_\delta k_\alpha & M_q + M_\delta k_q & M_\delta k_e \\ 1 & 0 & 0 \end{bmatrix} \begin{bmatrix} \alpha_m \\ q_m \\ e_{Im} \end{bmatrix} + \begin{bmatrix} 0 \\ 0 \\ -1 \end{bmatrix} \delta_c, \tag{3.12}$$

or, compactly, $\dot{x_m} = A_m x + b_m\delta_c$. The feedback gain, k_x, is found as before by minimizing the cost function in (3.5) subject to the dynamics in (3.11) with no parameter uncertainty. A suitable closed loop response was found with $Q = diag([\ 1 \quad 1 \quad 10\ ])$ and $R = 1$ to give the feedback gains $k_x = [\ 1.2996 \quad 0.5305 \quad 3.1623\ ]^T$. The controller described above was applied to the nonlinear aircraft. Figures 3-8 and 3-9 show the response of the closed loop system without uncertainty (dashed line) to an elevator doublet.

3.6 Adaptive Augmentation and RLAS

The system in (3.11) is augmented with adaptation as in (2.4) and(2.6), using the state error vector $e = [\ (\alpha - \alpha_m) \quad (q - q_m) \quad (e_I - e_{Im})\ ]^T$. The resulting error dynamics can be expressed

$$\begin{bmatrix} \dot{e} \\ \dot{\tilde{\theta}} \end{bmatrix} \begin{bmatrix} A_m & \lambda_\delta b\omega^T \\ -\Gamma\omega b^T P & 0 \end{bmatrix} \begin{bmatrix} e \\ \tilde{\theta} \end{bmatrix}, \tag{3.13}$$

where ω and $\tilde{\theta}$ are as defined previously in (2.5). As before, the reference model is chosen to be the closed-loop dynamics without uncertainty as in (3.12). The RLAS of the closed loop aircraft with optimal PI controller and adaptive augmentation can be seen directly from (2.15) and(3.13) to be

$$\begin{bmatrix} \dot{e_a} \\ \dot{\tilde{\delta}}_a \end{bmatrix} \begin{bmatrix} \left(A_m + \lambda_\delta b\theta_{x_c}^T\right) & \lambda_\delta b \\ -\gamma b^T P & 0 \end{bmatrix} \begin{bmatrix} e_a \\ \tilde{\delta}_a \end{bmatrix}, \tag{3.14}$$

where $\gamma = \omega_{mc}^T$, and ω_{mc} and θ_{xc} are as defined previously.

3.7 Design and Verification Procedure

As before, the design task was to provide adaptive augmentation while still meeting the military specification for short period frequency and damping (3.10). The design procedure described in section 2.5 was employed. It was found that for $G = 100diag([\ 1\ \ 1\ \ 1\ \ 1\ \ 0.0035\ ])$ and $Q = diag([\ 10\ \ 0.5\ \ 0.5\ ])$ the RLAS had a second order mode with damping ratio $\zeta = 0.492$, and natural frequency $\omega_n = 1.48rad/s$, and 1^{st} order modes with time constants $t_1 = 0.294s$ and $t_2 = 124.8s$. The second 1^{st} order mode, although it is slow, has no noticeable adverse effect on the RLAS response.

A moderate failure and a severe failure were simulated with the nominal and adaptive controllers to compare their performance (see figs. 3-8 through 3-11). The moderate failure, parameterized by $\lambda_\alpha = \lambda_q = 1$, $\lambda_\delta = 0.5$, $d_{trm} = 0.1563$, and the severe failure, parameterized by $\lambda_\alpha = -0.226$, $\lambda_q = -0.470$, $\lambda_\delta = 0.5$, $d_{trm} = 0.2623$, were introduced at $t = 7s$. It was observed that the performance of the adaptive system (solid line) was similar to that of the nominal LQ controller (dotted line) for the moderate failure, but for the severe failure, the adaptive augmented system maintained stability and tracking while the system without adaptation diverged. This shows that the adaptive controller clearly outperforms the nominal controller.

The severe failure in figs. 3-10 and 3-11 was explored more carefully for the purposes of verification. Figures 3-12 and 3-13 show the α and q response of the adaptive system to a random amplitude square-wave input for the severe failure. After a transients of about five seconds, adequate model following is achieved for α. For q, the unmodeled phugoid mode can be clearly observed in the q trajectory of the nonlinear aircraft. The phugoid mode for this aircraft has a frequency of $\omega_n = 0.122rad/s$ corresponding to a cycle time of $51.5s$, which agrees closely with the low frequency oscillations observed in fig. 3-13. The model mismatch due to the phugoid mode could be easily eliminated by using a more sophisticated longitudinal

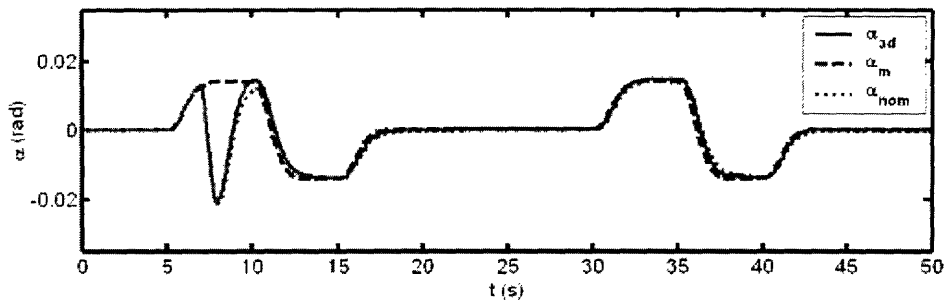

Figure 3-8: The α response of the LQ controller (nom) and the adaptive augmented controller (ad) to two elevator doublets are shown for a moderate failure occurring at $t = 7s$. The failure is parameterized by $\lambda_\alpha = \lambda_q = 1$, $\lambda_\delta = 0.5$, $d_{trm} = 0.1563$. For the moderate failure, the responses of the two systems are similar.

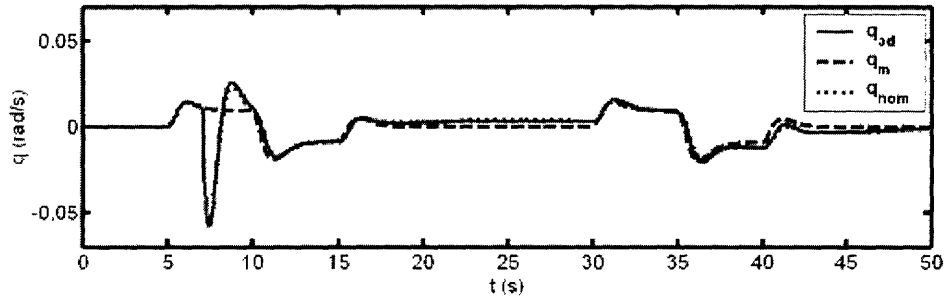

Figure 3-9: The q response of the LQ controller (nom) and the adaptive augmented controller (ad) to two elevator doublets are shown for a moderate failure occurring at $t = 7s$. The failure is parameterized by $\lambda_\alpha = \lambda_q = 1$, $\lambda_\delta = 0.5$, $d_{trm} = 0.1563$. For the moderate failure, the responses of the two systems are similar.

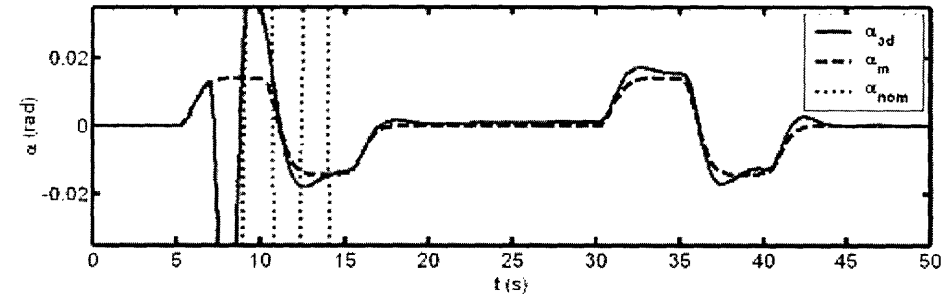

Figure 3-10: The α response of the LQ controller (nom) and the adaptive augmented controller (ad) to two elevator doublets are shown for a severe failure occurring at $t = 7s$. The failure is parameterized by $\lambda_\alpha = -0.226$, $\lambda_q = 0.470$, $\lambda_\delta = 0.5$, $d_{trm} = 0.2623$. For the severe failure, the system with the LQ controller becomes unstable, while the adaptive augmented systems maintains stability and tracking.

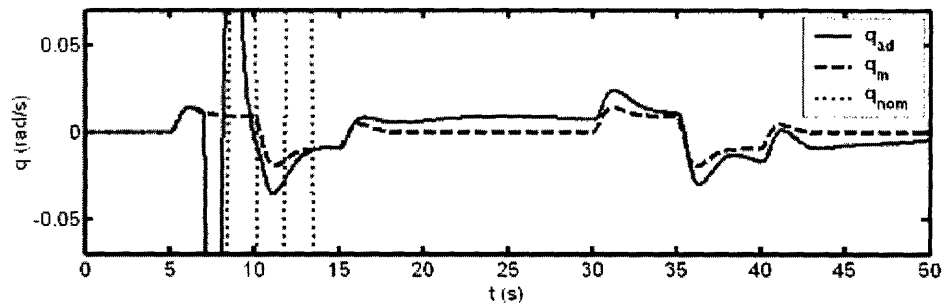

Figure 3-11: The q response of the LQ controller (nom) and the adaptive augmented controller (ad) to two elevator doublets are shown for a severe failure occurring at $t = 7s$. The failure is parameterized by $\lambda_\alpha = -0.226$, $\lambda_q = 0.470$, $\lambda_\delta = 0.5$, $d_{trm} = 0.2623$. For the severe failure, the system with the LQ controller becomes unstable, while the adaptive augmented systems maintains stability and tracking.

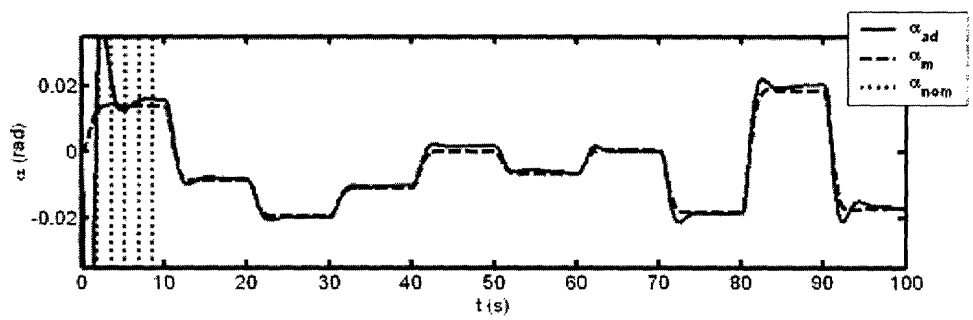

Figure 3-12: The α trajectory of the adaptive augmented system is shown with uncertainties parameterized by $\lambda_\alpha = -0.226$, $\lambda_q = 0.470$, $\lambda_\delta = 0.5$, $d_{trm} = 0.2623$. The RLAS was used to design a suitable adaptive response to a random amplitude square-wave input. The trajectories of the reference model and the nominal system are shown for comparison. Note that the nominal system is unstable.

reference model, namely one including phugoid dynamics. This exercise demonstrates that even with the crudest of plant models an adaptive controller with adequate transient properties can be realized using the RLAS.

The verification procedure described in section 2.5 was carried out for the severe failure. Figures 3-14 and 3-15 show in detail the first five seconds of the response in comparison to the RLAS. During the transient period, although the RLAS does not track the nonlinear system closely, its frequency of oscillation provides a good representation of the oscillations of the nonlinear aircraft. As the adaptive system evolves, the RLAS provides a more accurate representation of its trajectory (see figs.

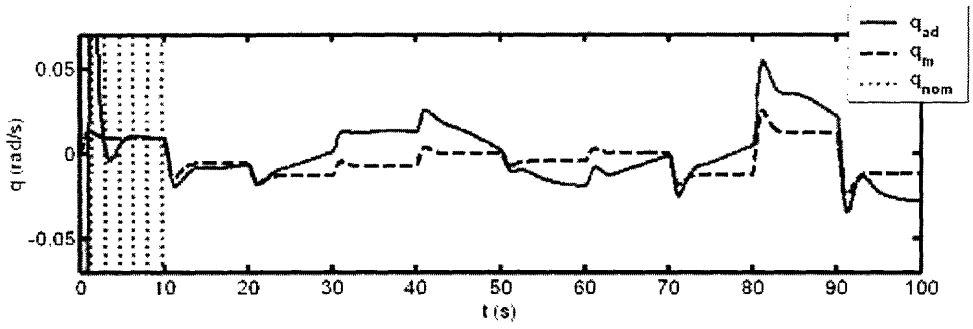

Figure 3-13: The q trajectory of the adaptive augmented system is shown with uncertainties parameterized by $\lambda_\alpha = -0.226$, $\lambda_q = 0.470$, $\lambda_\delta = 0.5$, $d_{trm} = 0.2623$. The low frequency oscillations in the q trajectory are from the unmodeled phugoid mode of the nonlinear aircraft. The RLAS was used to design a suitable adaptive response to a random amplitude square-wave input. The trajectories of the reference model and the nominal system are shown for comparison. Note that the nominal system is unstable.

3-16 and 3-17). Again, the offset of the nonlinear system in fig. 3-17 is attributed to the unmodeled phugoid mode. It is clear that the RLAS tracks the adaptive system relatively closely even for the nonlinear aircraft model.

It should be stressed, as well, that the closed loop trajectory is that of a full nonlinear aircraft model with an LQ controller and an adaptive controller. Thus the system is highly nonlinear, yet its qualities of oscillation can be inferred from the simple linear RLAS to a practically useful degree. Figures 3-14 through 3-17 verify that the adaptive system response is within the military flying qualities specification (3.10) as expected from the RLAS design procedure.

3.8 Summary

In this chapter the RLAS was used to design an adaptive augmented control system in two realistic examples from flight mechanics. The RLAS techniques were used with a linear model of short period dynamics. The adaptive system was verified to have properties that meet military specifications. The same design techniques were then applied to a nonlinear 6-DOF aircraft simulation. Again, it was demonstrated that an adaptive controller can be tuned to meet military specifications using the RLAS.

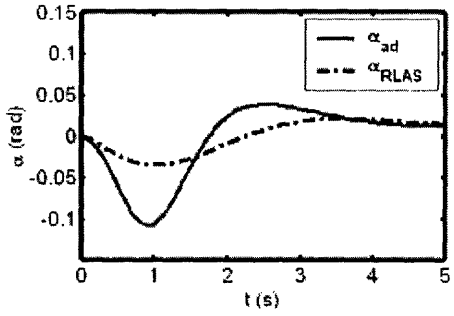

Figure 3-14: The α trajectory from fig. 3-12 is shown here in detail from $t = 0s$ to $t = 5s$. The RLAS (dash-dot) gives a good indication of the adaptive response frequency (solid) initially. The RLAS was designed to have a response well within military flying qualities specifications.

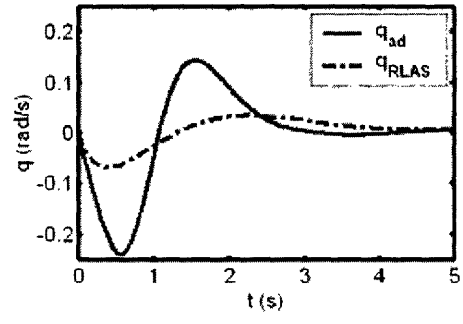

Figure 3-15: The q trajectory from fig. 3-13 is shown here in detail from $t = 0s$ to $t = 5s$. The RLAS (dash-dot) gives a good indication of the adaptive response frequency (solid) initially. The offset in the q trajectory is from the unmodeled phugoid mode. The RLAS was designed to have a response well within military flying qualities specifications.

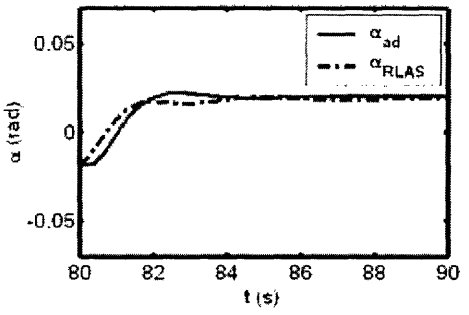

Figure 3-16: The α trajectory from fig. 3-12 is shown here in detail from $t = 80s$ to $t = 85s$. The RLAS (dash-dot) tracks the adaptive response (solid) well after transients have died out. The RLAS was designed to have a response well within military flying qualities specifications.

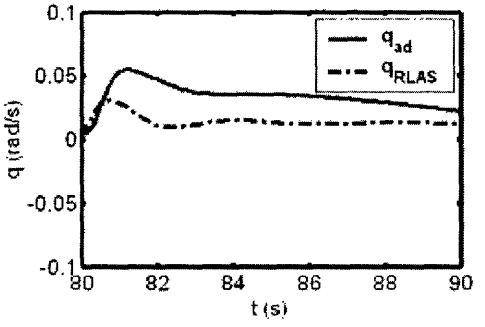

Figure 3-17: The q trajectory from fig. 3-13 is shown here in detail from $t = 0s$ to $t = 5s$. The RLAS (dash-dot) tracks the adaptive response (solid) well after transients have died out. The offset in the q trajectory is from the unmodeled phugoid mode. The RLAS was designed to have a response well within military flying qualities specifications.

Chapter 4

Saturation Constraints on Multiple Inputs

4.1 Introduction

In this chapter, we develop an extension of the result in [20] to multivariable plants. The technique proposed in [20] consists of modifying the error signal used for training adaptive gains so as to remove the effects of saturation from the error, and will be denoted in this chapter as Training Signal Hedging (TSH) as in [23]. The proof methodology for the multi-input case is quite similar to the single input case, though there are features that require significant modification. As in [20], we provide a region of initial conditions for which bounded trajectories are guaranteed for a multi-input adaptive system with magnitude-constrained inputs. This region is shown to extend to the entire state space if the plant is open-loop stable.

This chapter is organized as follows: In section 4.2 we review the proof strategy used in [20] and present the proof for a scalar plant. In section 4.3 we pose the multi-input problem, state the stability result in a theorem, and provide a proof. Section 4.4 contains simulation results, and a summary is presented in section 4.5.

4.2 Review of the First Order Case

It is valuable to gain a qualitative understanding of how TSH works as this will lead to insights in the course of proving the multi-input case. The approach in [20] uses a modified adaptive law in which the error signal used to adjust the control parameters is augmented so as to remove the part of the error that is due to saturation and retain the part that is due to a genuine mismatch between the plant and the reference model. The proof of stability ensures that this modification does not lead to a destabilizing action. The proof is reviewed below for the scalar case to acquaint the reader with the proof strategy.

A first order plant with measurable state is described by the equation

$$\dot{x} = a_p x + b_p sat\,(u) \tag{4.1}$$

where $a_p \in \Re$ and $b_p \in \Re^+$ are known, and where the $sat\,(.)$ function is given by

$$sat\,(u) = \begin{cases} u & if \quad |u| \leq u_{max} \\ u_{max} sgn\,(u) & if \quad |u| > u_{max} \end{cases}, \tag{4.2}$$

and where $u_{max} \in \Re^+$ is a known constant. A reference model is described by the first order differential equation

$$\dot{x}_m = -a_m x_m + b_m r_m \tag{4.3}$$

where $a_m \in \Re^+$ and $b_m \in \Re$ are known constants and r is a known bounded function so that

$$|r| \leq r_{max},$$

and $r_{max} \in \Re^+$ is a known constant. The reference model is chosen so that its state is the desired state of the plant.

We seek a control law, $u(t)$, such that all the signals in the system remain bounded and the error, $e = x - x_m$ is as small as possible. A standard feedback/feedforward

controller structure is chosen as

$$u(t) = k_x(t)x(t) + k_r(t)r(t). \tag{4.4}$$

Define the ideal control gains, k_x^* and k_r^*, such that

$$a_p + b_p k_x^* = -a_m \quad \text{and} \quad b_p k_r^* = b_m,$$

and define the parameter errors to be

$$\tilde{k}_x = k_x - k_x^* \quad \text{and} \quad \tilde{k}_r = k_r - k_r^*. \tag{4.5}$$

Then subtracting (4.3) from (4.1) and substituting with (4.4) and (4.5), the closed-loop error dynamics can be written

$$\dot{e} = -a_m e + b_p \tilde{k}_x x + b_p \tilde{k}_r r + b_p \Delta u,$$

where $\Delta u = u - sat(u)$ is the so called control deficiency signal. It is assumed that this signal can be measured or reconstructed from available measurements. The effects of saturation can be removed by treating Δu as an input disturbance, which can be removed from the training signal, e, by generating a signal e_Δ given by

$$\dot{e}_\Delta = -a_m e_\Delta + k_\Delta \Delta u,$$

with initial condition $e_\Delta(t_0) = 0$. Then the augmented error is defined as $e_u = e - e_\Delta$, which results in an augmented error dynamics given by

$$\dot{e}_u = -a_m e_u + b_p \tilde{k}_x x + b_p \tilde{k}_r r + \tilde{k}_\Delta \Delta u, \tag{4.6}$$

where $\tilde{k}_\Delta = b_p - k_\Delta$. Equation (4.6) is in a standard form for adaptive control, so we

give the adaptive laws as described in [27] and [34] as

$$\dot{k}_x = -\gamma_x e_u x, \quad \dot{k}_r = -\gamma_r e_u r, \text{ and } \quad \dot{k}_\Delta = -\gamma_\Delta e_u \Delta u, \tag{4.7}$$

where γ_x, γ_r, $\gamma_\Delta > 0$.

Consider the Lyapunov function candidate

$$V = \frac{1}{2}e^2 + \frac{1}{2}\frac{b_p}{\gamma_x}\tilde{k}_x^2 + \frac{1}{2}\frac{b_p}{\gamma_r}\tilde{k}_r^2 + \frac{1}{2}\frac{b_p}{\gamma_\Delta}\tilde{k}_\Delta^2.$$

Taking the time derivative along the trajectories of (4.6) and (4.7) leads to $\dot{V} \leq 0$, which implies that e_u, $\tilde{k}_x$, $\tilde{k}_r$, and $\tilde{k}_\Delta$ are bounded. Define k_{max} such that $k_{max} = max\left(sup|\tilde{k}_x|, sup|\tilde{k}_r|\right)$. Now define the following for notational efficiency:

$$\gamma_{max} = max(\gamma_x, \gamma_r),$$

$$x_{min} = \frac{b_p r_{max}\left(|k_r^*| + k_{max}\right)}{a_m - b_p k_{max}},$$

$$x_{max} = \frac{b_p u_{max}}{|a_p|}, \text{ and}$$

$$\bar{k}_{max} = \frac{a_m - |a_p||k_r^*|\frac{r_{max}}{u_{max}}}{b_p + |a_p|\frac{r_{max}}{u_{max}}}.$$

Theorem 4.1 *For the plant in (4.1) with the controller in (4.4) and the adaptive laws in (4.7), $x(t)$ has bounded trajectories for all $t \geq t_0$ if*

i) $|x(t_0)| < x_{max}$, *and*

ii) $\sqrt{V(t_0)} < \sqrt{\frac{b_p}{2\gamma_{max}}}\bar{k}_{max}$.

Further, $|x(t)| < x_{max}$ $\forall t \geq t_0$, and the error, e, is given by

$$|e(t)| = O[\sup_{\tau \leq t} \Delta u(\tau)].$$

Proof:

Let a positive definite function W be defined as

$$W(x) = \frac{1}{2}x^2,$$

and define an annulus region A as

$$A : \{x | x_{min} < |x| \leq x_{min}\},$$

where x_{min} and x_{max} are defined previously. Condition (ii) in Theorem 4.1 implies that $k_{max} < \bar{k}_{max}$. After substituting the definition for $\bar{k}_{max}$ and rearranging, we find that this leads to $x_{min} < x_{max}$, thus A is non-empty.

Next we show $\dot{W} < 0 \ \forall x \in A$ by considering two cases, case A, where $\Delta u = 0$, and case B, where $\Delta u \neq 0$. After this is established, we note that condition (i) in Theorem 4.1 implies that $W(x(t)) < W(x(t_0)) \ \forall t \geq t_0$. Theorem 4.1 follows directly.

Case A: $\Delta u = 0$

From (4.1), (4.4), and (4.5) we have

$$\dot{x} = -a_m x + b_p k_r^* r + b_p \tilde{k}_x x + b_p \tilde{k}_r r,$$

which leads to

$$\dot{W} = (-a_m x + b_p \tilde{k}_x)x^2 + b_p k_r^* r x + b_p \tilde{k}_r r x.$$

Bounding quantities on the right hand side gives

$$\dot{W} < (b_p k_{max} - a_m)|x|^2 + (b_p |k_r^*| r_{max} + b_p k_{max} r_{max})|x|.$$

Since $k_{max} < \bar{k}_{max}$ we have from the definition of $\bar{k}_{max}$ that $b_p k_{max} - a_m < 0$. We know then that

$$|x| < \frac{b_p r_{max}(|k_r^*| + k_{max})}{a_m - b_p k_{max}} \text{ implies } \dot{W} < 0.$$

Therefore, from the definition of x_{min}, we conclude that

$$\dot{W} < 0 \qquad \forall x \in A \text{ in case A.} \tag{4.8}$$

Case B: $\Delta u \neq 0$

We proceed by considering two sub-cases.

Sub-case(i): $sgn(u) = -sgn(x)$

From (4.1) and (4.2) we have

$$\dot{x} = a_p x + b_p sgn(u) u_{max},$$

which leads to

$$\dot{W} = a_p x^2 + b_p sgn(u) u_{max} x.$$

Based on the condition for sub-case(i) we can bound the right hand side as

$$\dot{W} \leq |a_p||x|^2 - b_p u_{max}|x|,$$

which, from the definition of x_{max}, leads to

$$|x| < x_{max} \text{ implies } \dot{W} < 0.$$

Therefore we conclude that

$$\dot{W} < 0 \qquad \forall x \in A \text{ in case B, sub-case } (i). \tag{4.9}$$

Sub-case(ii): $sgn(u) = sgn(x)$

From(4.1), (4.2), and (4.5) we have

$$\dot{x} = -a_m x - b_p k_x^* x + b_p sgn(u) u_{max},$$

which leads to

$$\dot{W} = -a_m x^2 - b_p k_x^* x^2 + b_p sgn(u) u_{max} x.$$

The condition for subcase (ii) implies that

$$b_p u x > b_p sgn(u) u_{max} x.$$

Substituting for u from (4.4) and(4.5) gives

$$b_p(\tilde{k}_x x + k_x^* x + k_r r)x > b_p sgn(u) u_{max} x.$$

We can move the k_x^* term to the right hand side and add $-a_m x^2$ to both sides to create $\dot{W}$ on the right, so that

$$-a_m x^2 + b_p \tilde{k}_x x^2 + b_p k_r r x > \dot{W}.$$

Bounding terms on the left hand side gives

$$(b_p k_{max} - a_m)|x^2| + (b_p k_{max} r_{max} + b_p |k_r^*| r_{max})|x| > \dot{W}.$$

From case A we saw that $b_p k_{max} - a_m < 0$, so from the definition of x_{min} we have that

$$x > x_{min} \text{ implies } \dot{W} < 0.$$

Therefore we conclude that

$$\dot{W} < 0 \qquad \forall x \in A \text{ in case B, sub-case } (ii). \tag{4.10}$$

From (4.8), (4.9), and (4.10) we have that

$$\dot{W} < 0 \qquad \forall x \in A.$$

∇

4.3 Formulation for a Multi-Input Plant

We now generalize the result of the last section to include state-accessible plants with multiple inputs. Consider a plant model of the form

$$\dot{x} = A_p x + B_p \Lambda E_s(u) + B_p \Lambda f, \tag{4.11}$$

where $x \in \Re^n$ is the fully measurable state vector and $u \in \Re^m$ is the input vector. Also, $A_p \in \Re^{n \times n}$ is *unknown*, $B_p \in \Re^{n \times m}$ is *known*, $\Lambda \in \Re^{m \times m}$ is *unknown* and diagonal with positive entries, and $f \in \Re^m$ is *unknown*. The requirement that B_p is known with Λ unknown can be replaced by a completely unknown B_p, but the complication of the resulting adaptive controller obscures the main stability result. The function $E_s(.)$ is an elliptical multi-dimensional saturation function defined by

$$E_s(u) = \begin{cases} u & if \quad \|u\| \leq g(u) \\ \bar{u} & if \quad \|u\| > g(u) \end{cases} \tag{4.12}$$

where $g(u)$ is given by

$$g(u) = \left(\sum_{i=1}^{m} \left[\frac{\hat{e}_i}{u_{max_i}} \right]^2 \right)^{-1/2},$$

$\hat{e} = \frac{u}{\|u\|}$ denotes the unit vector in the direction of u, u_{max_i} is the saturation limit of the i^{th} actuator, and $\bar{u}$ is given by

$$\bar{u} = \hat{e} g(u). \tag{4.13}$$

The actuators saturate symmetrically in this formulation, though asymmetric saturation limits can be treated straightforwardly with the same approach. Two aspects of this saturation function should be noted. First, the function $g(u)$ returns the magnitude of the projection of u onto the boundary of the m-dimensional ellipsoid defined by $\|u\| = g(u)$, and hence $E_s(.)$ is denoted as an elliptical saturation function. Second, from (4.13) it is clear that the output of $E_s(.)$ is direction preserving (see fig. 4-1). The elliptical saturation function was used in this formulation for analytical

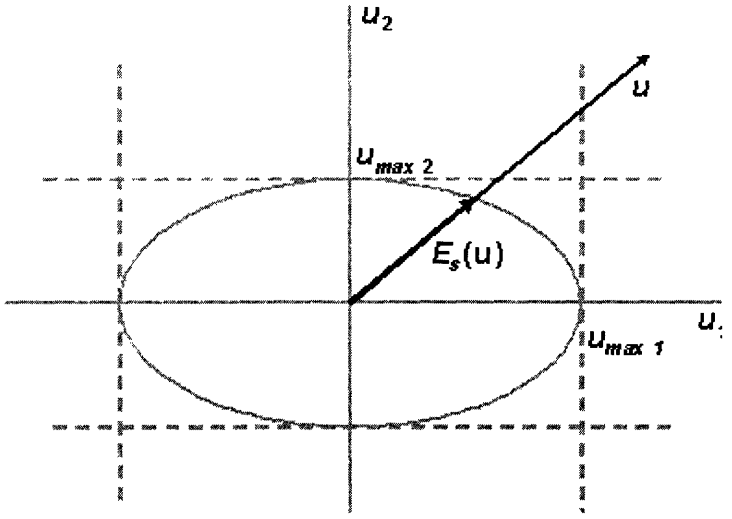

Figure 4-1: A schematic of the elliptical saturation function $E_s(.)$ for $m = 2$ is shown in this figure. Notice that it is direction preserving.

expediency. A more realistic rectangular saturation function will be discussed later.

A reference model whose state represents the desired sate of the plant is chosen as

$$\dot{x}_m = A_m x_m + B_m r \tag{4.14}$$

where $x \in \Re^n$, and $r \in \Re^l$ is a bounded reference input vector so that $\|r\| < r_{max}$. Note that r and u are not necessarily of the same dimension, therefore this architecture can be used for adaptive control allocation, as described in [31]. We also require that $A_m \in \Re^{n \times n}$ is Hurwitz, which is a standard requirement in adaptive control. The goal is to choose u so that $e = x - x_m$ is as small as possible, and all signals in the closed-loop systems remain bounded.

As before, a standard feedback/feedforward control structure is chosen as

$$u = K_x x + K_r r + k_f. \tag{4.15}$$

We assume that there exist ideal gain matricies $K_x^* \in \Re^{m \times n}$ and $K_r^* \in \Re^{m \times l}$, and an ideal constant vector $k_f^* \in \Re^m$ that results in perfect model following, so that $A_p + B_p \Lambda K_x^* = A_m$, $B_p \Lambda K_r^* = B_m$, and $B_p \Lambda (k_f^* + f) = 0$. Define the parameter errors

to be

$$\tilde{K}_x = K_x - K_x^*, \quad \tilde{K}_r = K_r - K_r^*, \text{ and } \quad \tilde{k}_f = k_f - k_f^*. \tag{4.16}$$

The subracting (4.14) from (4.11) and substituting with (4.15) and (4.16), the closed-loop error dynamics can be written

$$\dot{e} = A_m e + B_p \Lambda(\tilde{K}_x x + \tilde{K}_r r + \tilde{k}_f + \Delta u), \tag{4.17}$$

where $\Delta u = u - E_s(u)$ represents the control deficiency signal, as in the previous section. To eliminate the adverse effect of the dicturbance Δu, generate a signal e_Δ as

$$\dot{e}_\Delta = A_m e_\Delta + B_p diag(\hat{\lambda})\Delta u,$$

where $\hat{\lambda} \in \Re^m$ is a vector, the terms of which are the estimates of the diagonal terms of the unknown matrix Λ. The effects due to saturation can be removed from the error in (4.17) by defining the augmented error as $e_u = e - e_\Delta$, which can be written

$$\dot{e}_u = A_m e_u + B_p \Lambda(\tilde{K}_x x + \tilde{K}_r r + \tilde{k}_f) + B_p diag(\Delta u)\tilde{\lambda}, \tag{4.18}$$

where $diag(\tilde{\lambda}) = \Lambda - diag(\hat{\lambda})$, and exploiting the fact that $diag(\tilde{\lambda})\Delta u = diag(\Delta u)\tilde{\lambda}$.

Since (4.18) is in a standard form relevant to several adaptive systems, we choose the adaptive laws for adjusting the parameters K_x, K_r, k_f, and $\hat{\lambda}$ as

$$\begin{aligned} \dot{K}_x &= -\Gamma_x B_p^T P e_u x^T, & \dot{K}_r &= -\Gamma_r B_p^T P e_u r^T, \\ \dot{k}_f &= -\Gamma_f B_p^T P e_u, \quad \text{and} & \dot{\hat{\lambda}} &= \Gamma_\lambda diag(\Delta u) B_p^T P e_u, \end{aligned} \tag{4.19}$$

where $A_m^T P + P A_m = Q$, and Q, Γ_x, Γ_r, Γ_f, and Γ_λ are positive definite. Define a Lyapunov function candidate V as

$$V = e_u^T P e_u + Tr(\tilde{K}_x^T \Gamma_x^{-1} \Lambda \tilde{K}_x) + Tr(\tilde{K}_r^T \Gamma_r^{-1} \Lambda \tilde{K}_r) + \tilde{k}_f^T \Gamma_f^{-1} \Lambda \tilde{k}_f + \tilde{\lambda}^T \Gamma_\lambda^{-1} \tilde{\lambda}. \tag{4.20}$$

Since all Γ and Λ are positive definite, V is positive definite in e_u, $\tilde{K}_x$, $\tilde{K}_r$, $\tilde{k}_f$, and $\tilde{\lambda}$. Taking the time derivative along the system trajectories leads to $\dot{V} = -e_u^T Q e_u \leq 0$,

which implies that the signals e_u, $\tilde{K}_x$, $\tilde{K}_r$, $\tilde{k}_f$, and $\tilde{\lambda}$ are bounded. Define K_{max} so that

$$K_{max} = \max\left(sup\|\tilde{K}_x\|,\, sup\|\tilde{K}_r\|,\, sup\|\tilde{k}_f\|\right).$$

For efficiency of notation we define the following:

$$q_{min} = \min eig(Q), \quad p_{min} = \min eig(P), \quad p_{max} = \max eig(P),$$

$$\rho = \sqrt{\frac{p_{max}}{p_{min}}}, \quad \bar{u}_{min} = \min_i(u_{max_i}), \quad \bar{u}_{max} = \max_i(u_{max_i}),$$

$$P_b = \|PB_p\Lambda\|, \quad \max(eig(\Gamma_x), eig(\Gamma_r), eig(\Gamma_f), eig(\Gamma_\lambda)), \quad \lambda_{min} = \min eig(\Lambda).$$

All vector norms are Euclidean norms and the matrix norm P_B is the induced matrix norm, which has the property $\|PB_p\Lambda x\| \leq \|P_B\|\|x\|$. Also, define

$$\beta = \frac{P_B K_{max}}{\|K_x^*\| + K_{max}}, \tag{4.21}$$

$$a_0 = \frac{\bar{u}_{min} K_{max}}{\|K_x^*\| + k_{max}} - 2\|f\|, \tag{4.22}$$

$$x_{min} = \frac{3P_B K_{max}(r_{max}+1) + 3P_B\|K_r^*\|r_{max} + 2P_B\bar{u}_{max} + P_B\|k_f^*\|}{q_{min} - 3p_B k_{max}}, \tag{4.23}$$

$$x_{max} = \frac{P_B a_0}{|q_{min} - 3P_B\|K_x^*\||}, \text{ and} \tag{4.24}$$

$$\bar{K}_{max} = \frac{q_{min} - \frac{\rho}{a_0}\left(3\|K_r^*\|r_{max} + 2\bar{u}_{max} + \|k_f^*\|\right)|q_{min} - 2P_B\|K_x^*\||}{3P_B + 3\frac{\rho}{a_0}(r_{max}+1)\,|q_{min} - 2P_B\|K_x^*\||}. \tag{4.25}$$

Assumption 4.1 *$\bar{u}_{min}$ is such that $a_0 > 0$.*

Assumption 4.1 implies that there is a constraint on the size of the unknown disturbance $\|f\|$ given by

$$\|f\| < \frac{\bar{u}_{min} K_{max}}{2\left(\|K_x^*\| + K_{max}\right)}.$$

Theorem 4.2 *Under assumption 4.1, for the system in (4.11) with the controller in (4.15) and the adaptive laws in (4.19), $x(t)$ has bounded trajectories for all $t \geq t_0$ if*

i) $\|x(t_0)\| < x_{max}\frac{1}{\rho}$, and

ii) $\sqrt{V(t_0)} < \bar{K}_{max}\sqrt{\frac{\lambda_{min}}{\gamma_{max}}}$.

Further,

$$\|x(t)\| < x_{max} \quad \forall t \geq t_0,$$

and the output error e is of the order

$$\|e\| = O\left[\sup_{\tau \leq t} \|\Delta u(\tau)\|\right].$$

Proof:

We shall choose a positive definite function, $W(x)$, as

$$W = x^T P x \tag{4.26}$$

and define a level set, B, of W as

$$B : \left\{x | W(x) = p_{min} x_{min}^2\right\}, \tag{4.27}$$

where x_{max} is as defined in (4.24). Now define the annulus region A as

$$A : \{x | x_{min} < \|x\| \leq x_{max}\}, \tag{4.28}$$

where x_{min} is defined in (4.23). The proof proceeds in 2 steps. In step 1 we show that condition (ii) from theorem 4.2 implies that $B \subset A$. In step 2 we show that $\dot{W} < 0$ $\forall x \in A$. Condition (i) from theorem 4.2 implies that

$$W(x(t_0)) < W(B).$$

Therefore the results of step 1 and step 2 imply that

$$W(x(t)) < W(x(t_0)) \quad \forall t \geq t_0.$$

Theorem 4.2 follows directly.

Step 1:

In this step we show that $B \subset A$. First, from condition (ii) from theorem 4.2, it follows that $K_{max} < \bar{K}_{max}$. Substituting the expression for $\bar{K}_{max}$ leads to

$$\rho \frac{3K_{max}(r_{max}+1) + 3\|K_r^*\| r_{max} + 2\bar{u}_{max} + \|k_f^*\|}{q_{min} - 3P_B K_{max}} < \frac{a_0}{|q_{min} - 2P_B\|K_x^*\||}. \tag{4.29}$$

The inequality in (4.29) with the definition of x_{min} and x_{max} from (4.23) and (4.24) respectively directly implies

$$\rho x_{min} < x_{max}. \tag{4.30}$$

From (4.26), $W(x)$ can be bounded from below by $p_{min}\|x\|^2 \leq W(x)$, which implies from (4.27) that

$$\|x\| \leq x_{max} \quad \forall x \in B.$$

Likewise, from (4.26), $W(x)$ can be bounded from above by $W(x) \leq p_{max}\|x\|^2$, which implies from (4.30) and (4.27) that

$$x_{min} < \frac{1}{\rho} x_{max} \leq \|x\| \quad \forall x \in B.$$

From the definition of A in (4.28) we conclude therefore that $B \subset A$.

Step 2:

We now show that $\dot{W} < 0 \; \forall x \in A$.

Case A: $\|\Delta u\| = 0$

From (4.11), (4.12), and (4.16) we get

$$\dot{x} = A_m x + B_p \Lambda(\tilde{K}_x x + \tilde{K}_r r + \tilde{k}_f),$$

which leads to

$$\dot{W} = x^T(Q + 2PB_p\Lambda\tilde{K}_x)x + 2PB_p\Lambda(\tilde{K}_r r + K_r^* r + \tilde{k}_f)x.$$

Bounding quantities on the right hand side using previous definitions gives

$$\dot{W} < (2P_B K_{max} - q_{min})\|x\|^2 + 2P_B K_{max}(r_{max} + 1)\|x\| + 2P_B\|K_r^*\|r_{max}\|x\|.$$

From condition (ii) of theorem 4.2 and from the definition of K_{max} it follows that

$$K_{max} < \bar{K}_{max} < \frac{q_{min}}{3P_B}. \tag{4.31}$$

Therefore

$$\dot{W} < 0 \quad \text{if} \quad \|x\| > \frac{2P_B K_{max}(r_{max} + 1) + 2P_B\|K_r^*\|r_{max}}{(q_{min} - 2P_B K_{max})}.$$

The choice of x_{min} in (4.23) implies that

$$x_{min} > \frac{2P_B K_{max}(r_{max} + 1) + 2P_B\|K_r^*\|r_{max}}{(q_{min} - 2P_B K_{max})}.$$

Hence,

$$\dot{W} < 0 \qquad \forall x \in A \text{ in case A.} \tag{4.32}$$

Case B: $\|\Delta u\| \neq 0$

Equations (4.11), (4.12), (4.15), and (4.16) give

$$\dot{x} = A_m x - B_p \Lambda K_x^* x + B_p \Lambda \bar{u} + B_p \Lambda f. \tag{4.33}$$

Take the time derivative of (4.26) along the trajectories of (4.33) to get

$$\dot{W} = -x^T Q x - 2x^T P B_p \Lambda K_x^* x + 2x^T P B_p \Lambda(\bar{u} + f). \tag{4.34}$$

Sub-case(i): $2x^T P B_p \Lambda \bar{u} < -\bar{u}_{min}\beta\|x\|$

Using (4.34) and the condition for sub-case (i), and previously defined upper

bounds, we can bound $\dot{W}$ by

$$\dot{W} < \|x\|^2 \left|2P_B\|K_x^*\| - q_{min}\right| + \|x\|2P_B\|f\| - \|x\|\bar{u}_{min}\beta.$$

This implies that if

$$\|x\| \leq \frac{P_B a_0}{\left|q_{min} - 2P_B\|K_x^*\|\right|} \text{ then } \dot{W} < 0. \tag{4.35}$$

From the definition of x_{max} in (4.24), we have therefore that

$$\dot{W} < 0 \qquad \forall x \in A \text{ in case B, sub-case}(i). \tag{4.36}$$

Sub-case(ii): $2x^T P B_p \Lambda \bar{u} \geq -\bar{u}_{min}\beta\|x\|$

From (4.13), the condition for sub-case (ii) implies that

$$2x^T P B_p \Lambda \frac{u}{\|u\|}\|\bar{u}\| + \|x\|\bar{u}_{min}\beta \geq 0.$$

Substituting for u in (4.15), and for K_x from (4.16) gives

$$2x^T P B_p \Lambda \left(\tilde{K}_x x + K_r r + k_f\right) + \|x\|\bar{u}_{min}\beta\frac{\|u\|}{\|\bar{u}\|} \geq -2x^T P B_p \Lambda K_x^* x.$$

Adding terms to create $\dot{W}$ on the right hand side gives

$$\begin{aligned} -x^T Q x + 2x^T P B_p \left(\tilde{K}_x x + K_r r + k_f\right) + \\ \|x\|\bar{u}_{min}\beta\tfrac{\|u\|}{\|\bar{u}\|} + 2x^T P B_p \Lambda \bar{u} + 2x^T P B_p f \geq \dot{W}. \end{aligned}$$

Simplifying with (4.16),

$$\begin{aligned} -x^T Q x + 2x^T P B_p \left(\tilde{K}_x x + K_r r + \tilde{k}_f\right) + \\ \|x\|\bar{u}_{min}\beta\tfrac{\|u\|}{\|\bar{u}\|} + 2x^T P B_p \Lambda \bar{u} \geq \dot{W}, \end{aligned}$$

and using (4.25) and previous definitions to bound unknown quantities

$$\begin{gathered} -q_{min}\|x\|^2 + 2\|x\|P_B\left(K_{max}\|x\| + K_{max}r_{max} + \|K_r^*\|r_{max} + K_{max}\right) + \\ \|x\|\|u\|\beta + 2\|x\|P_B\bar{u}_{max} > \dot{W}. \end{gathered} \tag{4.37}$$

We note from (4.15) that

$$\|u\| \leq \left(\|K_x^*\| + K_{max}\right)\|x\| + \left(\|K_r^*\| + K_{max}\right)r_{max} + \left(\|f_f^*\| + K_{max}\right), \tag{4.38}$$

and from (4.21) that

$$0 \leq \beta \leq P_B. \tag{4.39}$$

Using (4.38) and(4.39) in (4.37) gives

$$\begin{gathered} \|x\|^2\left(3P_BK_{max} - q_{min}\right) + \|x\|\left(3P_BK_{max}(r_{max}+1) + 3P_B\|K_r^*\|r_{max}\right) + \\ \|x\|\left(2P_B\bar{u}_{max} + P_B\|k_f^*\|\right) > \dot{W}. \end{gathered} \tag{4.40}$$

Then, from (4.31) and (4.40) we know that

$$\|x\| > \frac{3P_BK_{max}(r_{max}+1) + 3P_B\|K_r^*\|r_{max} + 2P_B\bar{u}_{max} + P_B\|k_f^*\|}{q_{min} - 3P_BK_{max}}$$

implies that $\dot{W} < 0$. From the definition of x_{min} in (4.23), we have that

$$\dot{W} < 0 \qquad \forall x \in A \text{ in case B, sub-case}(ii). \tag{4.41}$$

From (4.32), (4.36), and(4.41) it follows that

$$\dot{W} < 0 \qquad \forall x \in A.$$

∇

Remark 4.1 *In the case of magnitude saturation, global stability is impossible for an unstable plant. Initial conditions can always be found to cause the plant state to become unbounded regardless of the controller. Thus any stability result for unstable*

plants must be local in nature, as the one presented in Theorems 4.1 and 4.2.

Remark 4.2 *In the case of an open loop stable plant, bounded trajectories are guaranteed for all initial conditions. If A_p is stable, (4.11) is BIBO stable, and (4.12) implies that $E_s(u)$ is bounded, therefore x is bounded.*

Remark 4.3 *Determining $\bar{u}$ in (4.12) can be computationally burdensome, especially for $m > 2$. A simpler and more intuitively compelling saturation function is given by $R_s(u)$, where the elements of Rs are defined by the ordinary saturation function*

$$R_{s_i} = sat(u_i) = \begin{cases} u_i & if \quad |u_i| \leq u_{max_i} \\ u_{max_i} sgn(u_i) & if \quad |u_i| > u_{max_i} \end{cases}, \tag{4.42}$$

$$for\ i = 1, ..., m.$$

This saturation function can be expressed as the sum of a direction preserving component and an error component, so that

$$R_s = \begin{cases} u & if \quad \|u\| \leq h(u) \\ u_d + \tilde{u} & if \quad \|u\| > h(u) \end{cases},$$

where $u_d = \hat{e}h(u)$. As before, $\hat{e}$ is the unit vector in the direction of u, and $h(u)$ returns the magnitude of the projection of u onto the hyper-rectangle defined by the saturation limits u_{max_i}, where $i = 1, ..., m$. In this formulation, u_d is in the same direction as u and $\tilde{u}$ is an error vector. Figure 2 illustrates the nature of $R_s(.)$ for the case when $m = 2$. It can be shown that $\tilde{u}$ is a bounded vector, whose bound depends upon the bound of the state x_{max}. This in turn causes the extension of the above proof to the case of rectangular saturation to become more complex, and is beyond the scope of this chapter. However, this case is treated in the simulation results in the next section, which show that for a rectangular saturation function, bounded trajectories can be achieved for a larger set of initial conditions than for the elliptical saturation function.

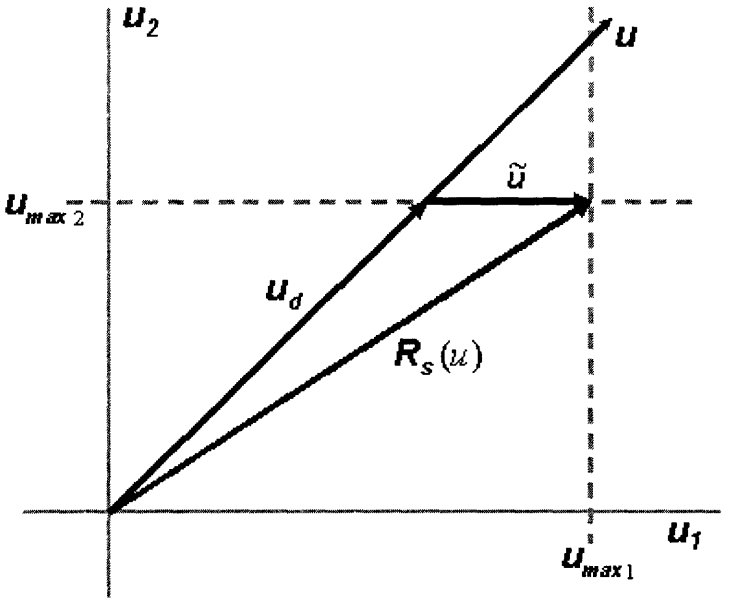

Figure 4-2: A schematic of the rectangular saturation function $R_s(.)$ for $m = 2$ is shown the figure. Notice that it is not necessarily direction preserving. That is $\tilde{u} \neq 0$ in general.

4.4 Simulations

Numerical simulations were carried out to demonstrate the usefulness of the proposed saturation compensation technique. An unstable, second order, two input plant in the form of (4.11) whose dynamics are given by

$$A_p = \begin{bmatrix} 1 & 1 \\ 0 & 1 \end{bmatrix}, B_p = \begin{bmatrix} 1 & 0 \\ 0 & 1 \end{bmatrix}, \Lambda = \begin{bmatrix} 1 & 0 \\ 0 & 1 \end{bmatrix}, \text{and } f = \begin{bmatrix} 0 \\ 0 \end{bmatrix} \tag{4.43}$$

was chosen for simulation. The reference model was selected in the form of (4.14) with dynamics given by

$$A_m = \begin{bmatrix} -1 & 1 \\ 0 & -2 \end{bmatrix}, B_m = \begin{bmatrix} 1 & 0 \\ 0 & 1 \end{bmatrix}.$$

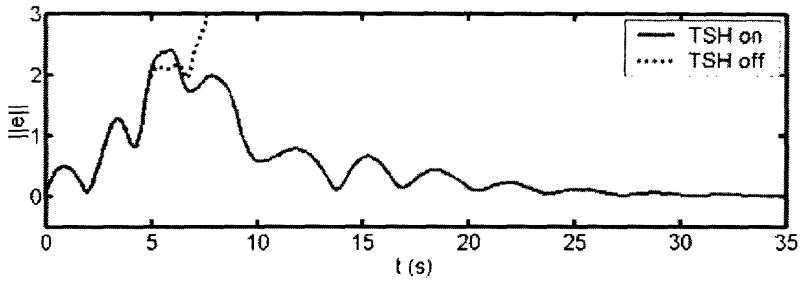

Figure 4-3: The L_2 norm of the tracking error is shown in this figure for the adaptive system with and without multi-input TSH. With TSH the error converges asymptotically to zero. Without TSH the error becomes unbounded.

The input, u, to the plant in (4.43) was constrained according to the rectangular saturation function $R_s(u)$ given in (4.42) where

$$u_{max_1} = u_{max_2} = 2.5.$$

All initial conditions were set to zero except for the initial value for $\hat{\lambda}(t)$, which was set to

$$\hat{\lambda}(t) = [\ 1 \quad 1\ ]^T.$$

A constant input r was given to the reference model at $t = 0$ where

$$r = [\ -1 \quad 1\ ]^T.$$

As stated previously, the task is for all signals in the adaptive system to remain bounded while the error, e, remains as small as possible.

Simulation results are shown in figs. 4-3 through 4-8. Figure 4-3 shows the L_2 norm of the tracking error for the adaptive system with and without multi-input TSH. It can be clearly seen that with TSH the tracking error converges to zero asymptotically, whereas without TSH the tracking error becomes unbounded.

The control input activity for the adaptive system with and without TSH is shown in figs. 4-4 and 4-5. With TSH (fig. 4-4), the controls saturate, but remain relatively well behaved. After $t = 10s$ the control signals remain within the saturation limits. Without TSH (fig. 4-5), both input signals saturate severely and go unbounded.

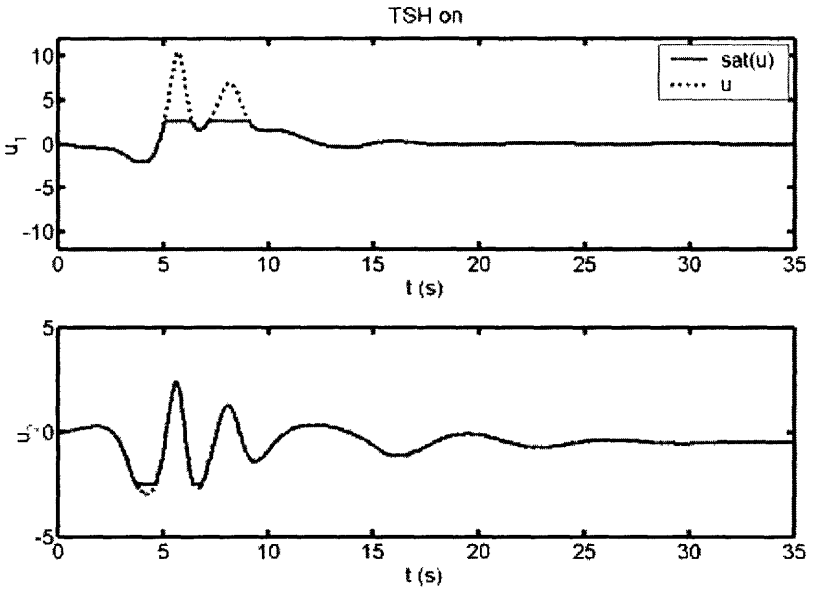

Figure 4-4: The control input activity is shown in this figure for the adaptive system with multi-input TSH. Saturation occurs initially for both inputs, however the control signal remains well behaved. After $t = 10s$ the control signal remains within the saturation limits.

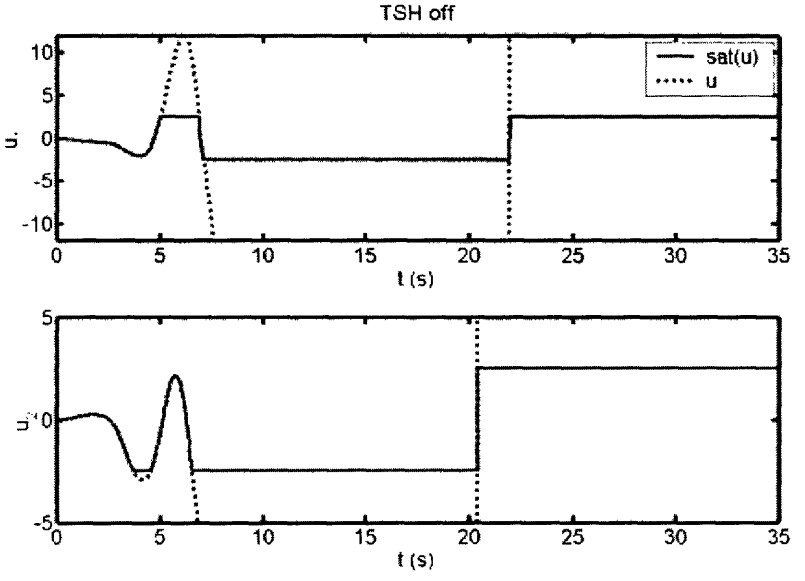

Figure 4-5: The control input activity is shown in this figure for the adaptive system without multi-input TSH. Both input signals saturate severely and become unbounded.

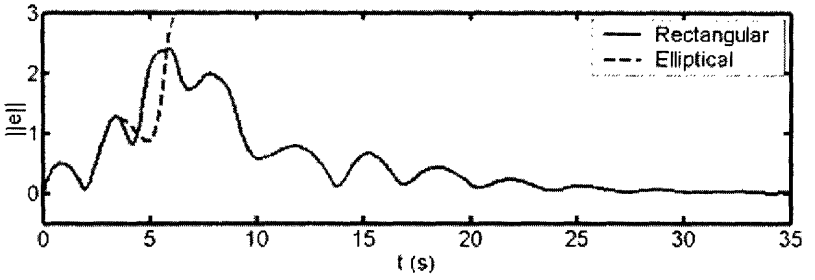

Figure 4-6: The L_2 norm of the tracking error is shown in this figure for the adaptive system with rectangular and elliptical saturation functions. With the rectangular function the error converges asymptotically to zero. With the elliptical function the error becomes unbounded.

As discussed in Remark 4.3, it is interesting to see in simulation the difference between the more realistic rectangular-type saturation function, $R_s(u)$, and the more analytically attractive elliptical saturation function, $E_s(u)$. The same simulation scenario described above was performed with the two saturation functions. Figure 4-6 shows that for the system with $R_s(u)$ the error converges to zero asymptotically, whereas with $E_s(u)$ the error becomes unbounded, demonstrating that $E_s(u)$ leads to a smaller region of initial conditions for which bounded trajectories are obtained.

Figures 4-7 and 4-8 show phase trajectories of the input signals for R_s and E_s. Partial outlines of the saturation boundaries can be seen in both cases. The input signal for the rectangular function (fig. 4-7) saturates intermittently, but settles within the saturation limits. The input signal with the elliptical function (fig. 4-8) saturates and becomes unbounded, again demonstrating that E_s leads to a smaller region of initial conditions for which bounded trajectories are obtained.

4.5 Summary

In this chapter, we have developed an extension of the approach in [20] to multivariable plants with magnitude-constrained inputs. It is shown that for initial conditions of the system state and the adaptive control parameters that lie inside a bounded region, bounded trajectories are guaranteed. This region is shown to extend to the entire state space if the plant is open-loop stable. This saturation compenstation tech-

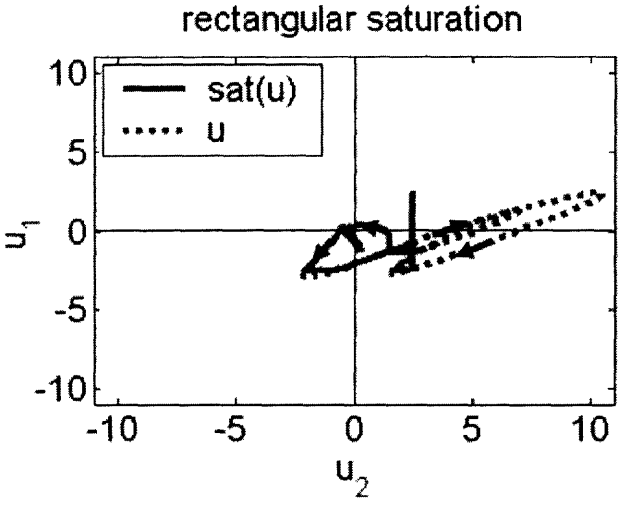

Figure 4-7: The input space is shown for the rectangular saturation function. The outlines of the rectangular saturation boundary is visible.

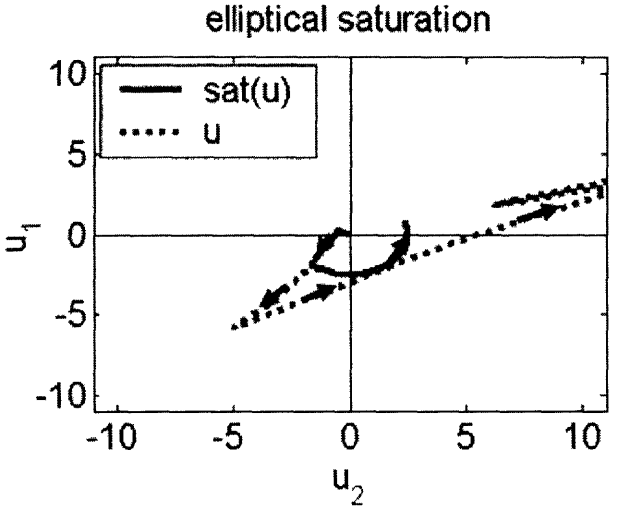

Figure 4-8: The input space is shown for the elliptical saturation function. The outlines of the ellitpical saturation boundary is visible.

nique will be incorporated in a realistic adaptive controller for aircraft reconfiguration in the next chatper.

Chapter 5

Application to Aircraft Reconfiguration

5.1 Introduction

In this chapter, we develop a controller for a realistic multiple-input aircraft model that simultaneously performs reconfiguration and control allocation by using a direct-adaptive approach. This strategy combines the benefits of both direct adaptive psuedo-control designs and indirect adaptive control allocating designs discussed in section 1.4, while avoiding the limitations of either. In addition, the proposed controller is able to suppress the adverse effects of actuator saturation by using the multi-input saturation compensation techniques developed in the previous chapter and in [32].

5.2 Problem Statement

We begin with a linearized model of a failed plant of the form

$$\dot{x} = A_p x + \Lambda B_p u + B_p f, \tag{5.1}$$

where $x \in \Re^n$ is the state vector, $u \in \Re^m$ is the input to the control actuators, $A_p \in \Re^{n \times n}$ is unknown, and $B_p \in \Re^{n \times m}$ is known. Actuator failures are represented by the unknown matrix $\Lambda \in \Re^{m \times m}$ and the unknown vector $f \in \Re^m$. Λ is a diagonal positive semi definite matrix with elements $0 \leq \lambda_i \leq 1$ for $i = 1, ..., m$. For each element, $\lambda_i = 0$ represents a complete failure of the corresponding actuator, $0 < \lambda_i < 1$ represents a class of partial actuator failures, and $\lambda_i = 1$ denotes a healthy actuator. The constant vector f accounts for the possibility that a failed actuator may be locked in an out-of-trim position. Additionally, the dynamics matrix A_p is considered to be unknown to account for two separate failure phenomena. First, if a nominal state feedback controller is in place prior to actuator failure, the feedback structure will cause A matrix changes in the event of failed actuators. Secondly, actuator failures may be accompanied by aerodynamic changes, which are expressed as uncertainties in the A matrix. Equation (5.1) can be considered as describing the dynamics of a perturbation about a known trimmed state. The state is assumed to be fully measurable, which is a common assumption and is reasonable given that modern aircraft are equipped with a large number of sensors [4].

In the case of reconfiguration after a failure, we can expect a vigorous utilization of the remaining operational actuators. It is therefore important to consider the effects of saturation on the system dynamics. We introduce multidimensional saturation into the model as

$$u = sat(u_c)$$

where the $sat(.)$ function is defined element-wise by

$$sat_i(u_{c_i}) = \begin{cases} u_{min_i} & if \quad u_i < u_{min_i} \\ u_i & if \quad u_{min_i} \leq u_i \leq u_{max_i} \\ u_{max_i} & if \quad u_i > u_{max_i} \end{cases}, \tag{5.2}$$

$$\text{for } i = 1, 2, ..., m,$$

and where the vectors u_{min} and u_{max} define the minimum and maximum position limits respectively of the m actuators. We have assumed that the effects of actuator

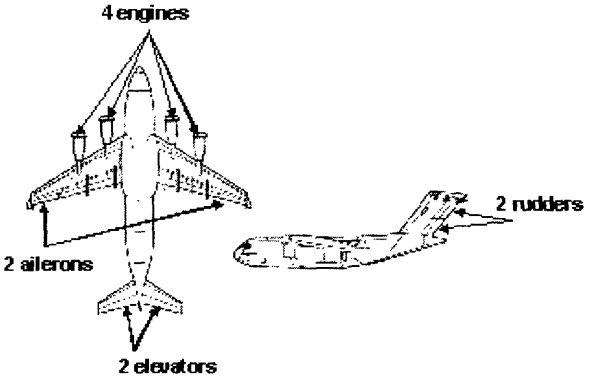

Figure 5-1: Redundant control actuators in an aircraft system are illustrated in this figure.

dynamics are negligible, which is a reasonable and common assumption for large, slowly maneuvering aircraft [4], [37].

The task of control allocation is to determine a suitable control input, u, given a pilot command, $r \in \Re^l$, where $l < m$. We therefore choose a reference model of the form

$$\dot{x}_m = A_m x_m + B_m r, \tag{5.3}$$

where $x_m \in \Re^n$, $r \in \Re^l$, $A_m \in \Re^{n \times n}$ is Hurwitz, and $B_m \in \Re^{n \times l}$, so that x_m represents the desired state plant. The goal is to choose u so that $e(t) = x - x_m$ is as small as possible, and all signals in the closed-loop system remain bounded.

In most flight control applications, control allocation methods are used to distribute pilot commands (or guidance and navigation law commands) among available aircraft control inputs. For example, a single pilot roll input can be allocated to produce a movement of two aileron panels, usually constrained to move anti-symmetrically. Actuator redundancies are introduced in the form of multiple aileron panels, rudder panels, elevator panels, and/or power plants (see figure 5-1).

5.3 Adaptive Controller

The controller we propose has a standard state-feedback/feedforward structure [27, 34]:

$$u_c = K_x x + K_r r + k_f. \tag{5.4}$$

We assume that there exist ideal gain matrices $K_x^* \in \Re^{m\times n}$ and $K_r^* \in \Re^{m\times l}$, and an ideal disturbance vector $k_f^* \in \Re^m$ that result in perfect model following, so that

$$A_p + B_p \Lambda K_x^* = A_m, \tag{5.5}$$

$$B_p \Lambda K_r^* = B_m, \tag{5.6}$$

$$B_p(\Lambda k_f^* + f) = 0. \tag{5.7}$$

Equations (5.5)-(5.7) are the so-called matching conditions for the adaptive system. The ideal gains need not be known; their existence is sufficient to show stability. Conditions (5.5) and (5.6) are standard in multivariable adaptive control [27, 34] and (5.7) is required because of the possible constant moment from a locked actuator. Tao et al [37], considered similar matching conditions in detail. In particular, situations in which the conditions are achievable and unachievable were investigated. Such matters will not be pursued here as this work is mostly concerned with the novelty of the control allocating design and the incorporation of a multi-input TSH technique.

Substituting (5.2) into (5.1) gives

$$\dot{x} = A_p x + B_p \Lambda u_c + B_p \Lambda \Delta u + B_p f, \tag{5.8}$$

where $\Delta u = u - u_c$ represents the control deficiency signal, as formulated in [20] and the previous chapter. Then, after substituting (5.4) into (5.8), simplifying using (5.5)-(5.7) and taking the difference with (5.3), the error dynamics of the system can be written

$$\dot{e} = A_m e + B_p \Lambda \left(\tilde{K}_x x + \tilde{K}_r r + \tilde{k}_f + \Delta u \right) \tag{5.9}$$

where

$$\tilde{K}_x = K_x - K_x^*,\ \tilde{K}_r = K_r - K_r^*, \text{ and } \tilde{k}_f = k_f - k_f^*.$$

TSH is implemented to compensate for the adverse effects of saturation. To this end, an auxiliary error is generated as in [20] and the previous chapter:

$$\dot{e}_\Delta = A_m e_\Delta + B_p diag(\hat{\lambda})\Delta u,$$

where $\hat{\lambda} \in \Re^m$ is a vector, the terms of which are the current estimates of the diagonal terms of the failure matrix Λ. The effects due to saturation can be removed from the error in (5.9) by defining the augmented error as $e_u = e - e_\Delta$, which can be written

$$\dot{e}_u = A_m e_u + B_p \Lambda \left(\tilde{K}_x x + \tilde{K}_r r + \tilde{k}_f \right) + B_p diag(\Delta u)\tilde{\lambda}, \tag{5.10}$$

where $diag(\tilde{\lambda}) = \Lambda - diag(\hat{\lambda})$, and exploiting the fact that $diag(\tilde{\lambda})\Delta u = diag(\Delta u)\tilde{\lambda}$.

Since (5.10) is in a standard form relevant to several adaptive systems, we choose the adaptive laws for adjusting the parameters K_x, K_r, k_f, and $\hat{\lambda}$ as

$$\dot{K}_x = -\Gamma_1 B_p^T P e_u x^T, \tag{5.11}$$

$$\dot{K}_r = -\Gamma_2 B_p^T P e_u r^T, \tag{5.12}$$

$$\dot{k}_f = -\Gamma_3 B_p^T P e_u, \tag{5.13}$$

$$\dot{\hat{\lambda}} = \Gamma_4 diag(\Delta u) B_p^T P e_u, \tag{5.14}$$

where $A_m^T P + P A_m = -Q$, $Q > 0$, and Γ_i is diagonal and positive definite for $i = 1, ..., 4$. The right hand side of equation (5.14) intentionally has the opposite sign of the others.

Define a Lyapunov function candidate V as

$$\begin{gathered} V = e_u^T P e_u + Tr\left(\tilde{K}_x^T \Gamma_1^{-1} \Lambda \tilde{K}_x \right) + Tr\left(\tilde{K}_r^T \Gamma_2^{-1} \Lambda \tilde{K}_r \right) + \\ \tilde{k}_f^T \Gamma_3^{-1} \Lambda \tilde{k}_f + \tilde{\lambda}^T \Gamma_4^{-1} \Lambda \tilde{\lambda}. \end{gathered} \tag{5.15}$$

Since Γ_i is diagonal, V is positive definite in e_u, $\Lambda\tilde{K}_x$, $\Lambda\tilde{K}_r$, $\Lambda\tilde{k}_f$, and $\tilde{\lambda}$. Taking the time derivative along the system trajectories leads to $\dot{V} = -e_u^T Q e_u \leq 0$, which implies that the signals e_u, $\Lambda\tilde{K}_x$, $\Lambda\tilde{K}_r$, $\Lambda\tilde{k}_f$, and $\tilde{\lambda}$ are bounded. We can define $\rho = \sqrt{\frac{p_{max}}{p_{min}}}$, and reformulate the result from the previous chapter to give

Theorem 5.1 *There exist positive scalars x_{max} and K_{max} such that for the system in (5.1), with the controller described in (5.4) and (5.11)-(5.14), $x(t)$ has bounded trajectories for all $t \geq t_0$ if*

i) $\|x(t_0)\| < x_{max}\frac{1}{\rho}$, *and*

ii) $\sqrt{V(t_0)} < K_{max}$.

Further,

$$\|x(t)\| < x_{max} \quad \forall t \geq t_0,$$

and the output error e is of the order

$$\|e\| = O\left[\sup_{\tau \leq t} \|\Delta u(\tau)\|\right].$$

Theorem 5.1 states what was found in the previous chapter and in [32], namely, that the controller in (5.4) guarantees that the closed-loop system has bounded solutions for a limited set of initial conditions. Note that the phrasing of theorem 5.1 is slightly different from the corresponding theorem in the previous chapter (theorem 4.2); specifically, it was simplified in this presentation to preserve the meaning without being obscured by details. Two theorems similar to theorem 5.1 are proved in [20], one for a scalar adaptive system and one for a single-input higher order adaptive system.

The above formulation of an adaptive reconfigurable flight controller has two principle improvements over other similar formulations. First, the controller does not rely on a fixed control allocation, and consequently the range of allowable actuator failures is expanded. In particular, previous direct-adaptive strategies have focused on designing $u_a \in \Re^l$, where

$$u_c = G u_a$$

and where $G \in \Re^{m \times l}$ is a fixed control allocation matrix. This requires that the failed system $(A_p, B_p \Lambda G)$ be controllable. The formulation in this chapter requires that $(A_p, B_p \Lambda)$ be controllable, which is a less restrictive requirement. Second, this formulation includes multivariable TSH, which, it was proved, will give bounded solutions for certain initial conditions. It should also be noted that recent extensions along the lines of [23] can be used to improve the transient performance of the adaptive system further.

5.4 Simulation Results

While the results presented in this paper are applicable to any system of the form (5.1) and (5.2), our focus is primarily on the 6 degree of freedom (6-DoF) aircraft dynamics. For this system, the state vector is of the form

$$x = [\ \alpha \quad q \quad \beta \quad p \quad r\ ]^T,$$

whose elements are the angle of attack, body pitch rate, angle of sideslip, body roll rate, and body yaw rate, respectively. The first two and the last three states are nearly decoupled in a linearized, trimmed system. We have implicitly used a common time-scale separation approximation. The 5 states considered here are typical of models of "fast" aircraft dynamics for stability augmentation, or "inner loop" control. The "slow" dynamics, consisting of airspeed, 3 Euler angles, and 3 earth referenced positions, are typically used in models for aircraft guidance and navigation, or "outer loop" control, and will not be considered here.

Using a linear model representative of a large transport aircraft [35], the direct-adaptive reconfigurable flight controller is designed according to the equations in (5.4) and (5.11)-(5.14). In this simulation $n = 5$, $m = 10$, and $l = 4$. The aircraft, has 4 power plants, 2 independent elevator panels, 2 independent aileron panels, and 2

States (x)	Description
α	Angle of Attack
q	Body Pitch Rate
β	Side Slip Angle
p	Roll Rate
r	Yaw Rate

Actuators (u)	Description	Saturation Limits $u_{i,min} = u_i = u_{i,max}$
t1	Left Outboard Throttle	$t1_{min} = -.4331$ $t1_{max} = .5669$
t2	Left Inboard Throttle	$t2_{min} = -.4331$ $t2_{max} = .5669$
t3	Right Inboard Throttle	$t3_{min} = -.4331$ $t3_{max} = .5669$
t4	Right Outboard Throttle	$t4_{min} = -.4331$ $t4_{max} = .5669$
e1	Left Elevator	$e1_{min} = -.2797rad$ $e1_{max} = .3313rad$
e2	Right Elevator	$e2_{min} = -.2797rad$ $e2_{max} = .3313rad$
a1	Left Aileron	$a1_{min} = -.436rad$ $a1_{max} = .436rad$
a2	Right Aileron	$a2_{min} = -.436rad$ $a2_{max} = .436rad$
r1	Lower Rudder	$r1_{min} = -.524rad$ $r1_{max} = .524rad$
r2	Upper Rudder	$r2_{min} = -.524rad$ $r2_{max} = .534rad$

Pilot Inputs (r)	Description
T	Virtual Throttle
E	Virtual Elevator
A	Virtual Aileron
R	Virtual Rudder

Table 5.1: Table showing the aircraft states, actuators with saturation limits, and pilot inputs used in the numerical simulations. Note that the saturation limits are expressed as variations from a trimmed position.

independent rudder panels. The input vector is defined as

$$u = [\ t1 \quad t2 \quad t3 \quad t4 \quad e1 \quad e2 \quad a1 \quad a2 \quad r1 \quad r1\ ]^T.$$

The states, actuator deflections, and pilot inputs are denoted as shown in table 5.1.

The matrices A_p, A_m, B_p, and B_m, the simulation initial conditions, and adaptive gains Γ_i and Q are shown in the appendix. The aircraft model is taken from a nonlinear 6-DoF aircraft simulation linearized at a speed of mach 0.3 and an altitude of 1000m. The reference model is chosen so as to decouple the aircraft roll and yaw desired dynamics. The performance of the closed loop adaptive system is compared with that of a nominal controller using a control law with the same structure as in (5.4), but with fixed gains K_{nom_x} and K_{nom_r} designed to achieve model following for the unfailed plant. The nominal gains are given in appendix A. The results of four

simulation runs with different control failures are shown in figures 5-2 through 5-7. Failure 1 shows a locked left elevator scenario, failure 2 corresponds to a locked left aileron, failure 3 represents a left outboard engine-out scenario, and failure 4 is a failed left elevator locked at full deflection. These failure scenarios are discussed in detail below.

5.4.1 Failure 1

Figures 5-2 and 5-3 show the results of a failed left elevator locked at 20% of its maximum upward deflection, which is represented as

$$\Lambda(5,5) = 0, \text{ and } f(5) = 0.2 \times e1_{min},$$

where negative elevator corresponds to upward deflection. The aircraft is commanded through two aggressive pitch doublets and the failure occurs at the beginning of the first maneuver at $t = 6$ seconds. With the nominal controller, the aircraft performance degrades quickly after the failure, as shown in figure 5-2. With the adaptive controller, the model is followed closely through the maneuvers after a transient of about 2 seconds. Figure 5-3 shows the control activity required to follow the model. In this example, the asymmetric elevator deflection due to failure causes a roll moment, which is compensated for by the ailerons. The lateral dynamics are not shown for the sake of brevity.

5.4.2 Failure 2

Figures 5-4 and 5-5 show the results of a failed left aileron locked at 40% downward deflection, represented as

$$\Lambda 7,7 = 0, \text{ and } f(7) = 0.4 \times a1_{max},$$

where positive left aileron corresponds to downward deflection. Similar to the previous case, the aircraft is commanded through two aggressive roll doublets and the failure

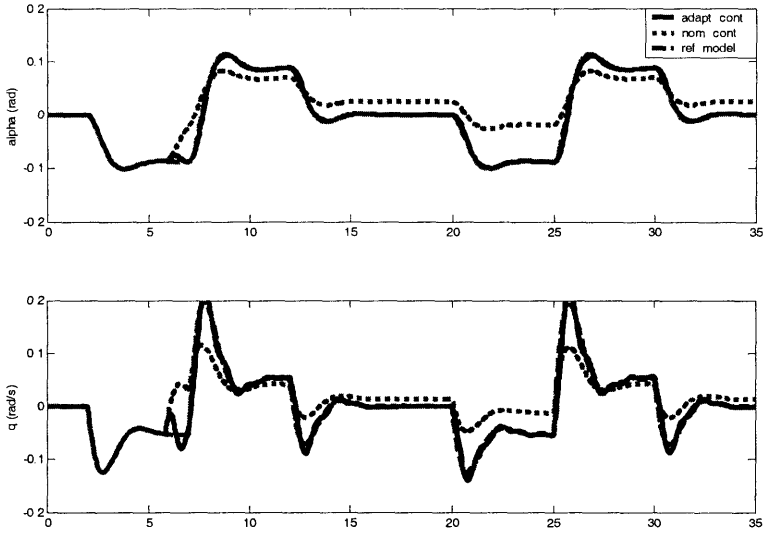

Figure 5-2: System response to failure 1, a failed left elevator locked at 20% of its upward travel, is shown. The aircraft is commanded through two aggressive pitch doublets and the failure occurs at $t = 6s$. Only the longitudinal states are shown.

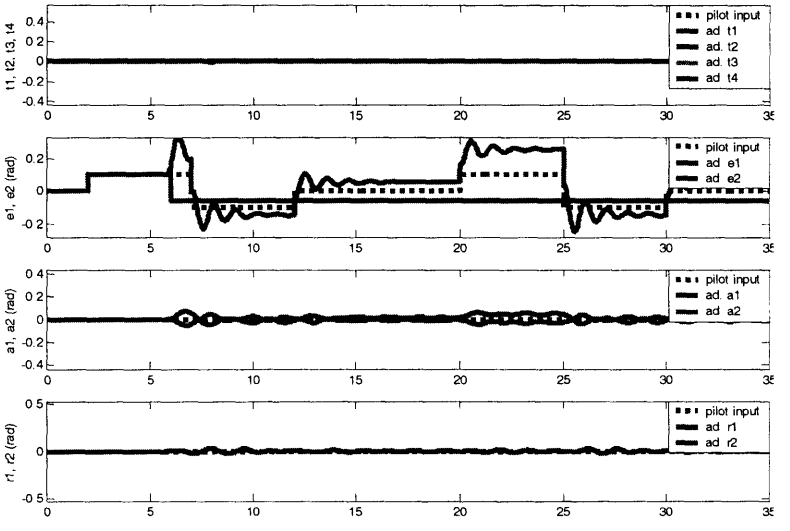

Figure 5-3: Actuator activity of the aircraft with failure 1, a failed left elevator locked at 20% of its upward travel, is shown. The aircraft is commanded through two aggressive pitch doublets and the failure occurs at $t = 6s$.

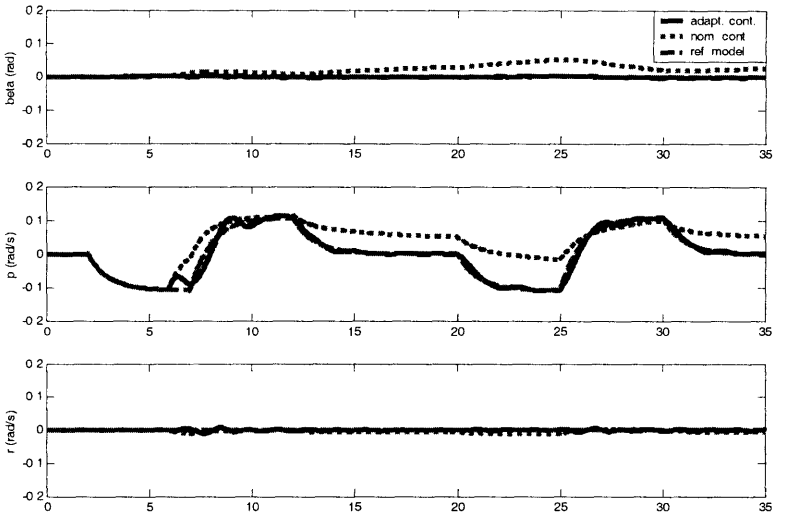

Figure 5-4: System response to failure 2, a failed left aileron locked at 40% of its downward travel. The aircraft is commanded through two aggressive roll doublets and the failure occurs at $t = 6s$. Only the lateral states are shown.

occurs at the beginning of the first maneuver at $t = 6$ seconds. The nominal controller causes the performance of the aircraft to degrade after the failure. The adaptive system, on the other hand, follows the model closely throughout the maneuver after a short transient. Notice that yaw and roll have been successfully decoupled, even in the presence of failure and saturation, as can be seen by the clipped aileron signal in figure 5-5. Also, it can be seen that the rudder must be actuated to achieve the yaw-roll decoupling, and the elevators are actuated anti-symmetrically to help produce the required roll moment.

5.4.3 Failure 3

Figures 5-6 and 5-7 show the results of a failed left outboard power plant giving zero thrust, which is represented as

$$\Lambda(1,1) = 0, \text{ and } f(1) = 1 \times t1_{min}.$$

In this case, the aircraft is commanded through two aggressive yaw doublets and, as before, the failure occurs at the beginning of the first maneuver at $t = 6$ sec-

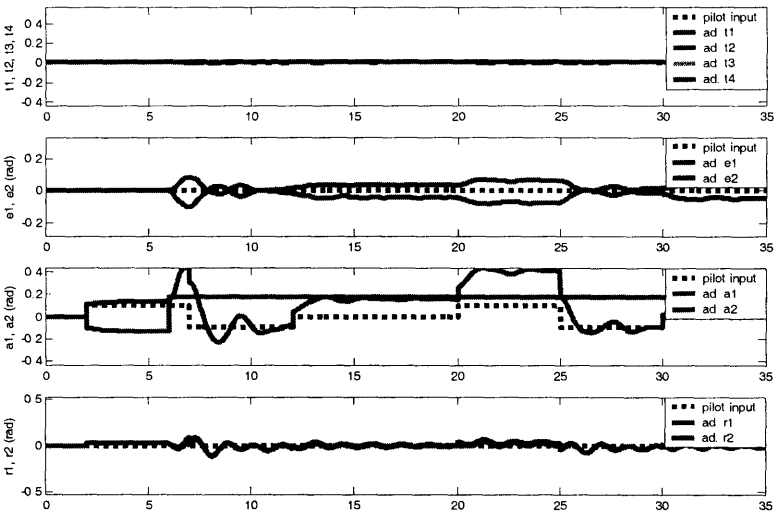

Figure 5-5: Actuator activity of the aircraft with failure 2, a failed left aileron locked at 40% downward travel. The aircraft is commanded through two aggressive roll doublets and the failure occurs at $t = 6s$

onds. Again, the nominal controller causes the aircraft trajectory to differ from the model, however the adaptive system follows the model despite failure. In addition, yaw and roll are successfully decoupled. The failed power plant creates a large yaw moment, which is counter acted by the rudders (see fig. 5-7). It should be noted that adaptive control with actuators with slow dynamics, such as power plants, should be undertaken cautiously. In these simulations, small adaptive gains, Γ_i, are used to discourage fast engine actuation (see appendix for Γ_i values), such that the commanded task does not exceed the engine bandwidth.

5.4.4 Failure 4

Figure 5-8 shows the stabilizing effect of the TSH in the presence of actuator saturation. The pitch rate and elevator deflections are shown for a failed left elevator locked at full upward deflection, which is represented as

$$\Lambda(5,5) = 0, \text{ and } f(5) = 1 \times e1_{min}.$$

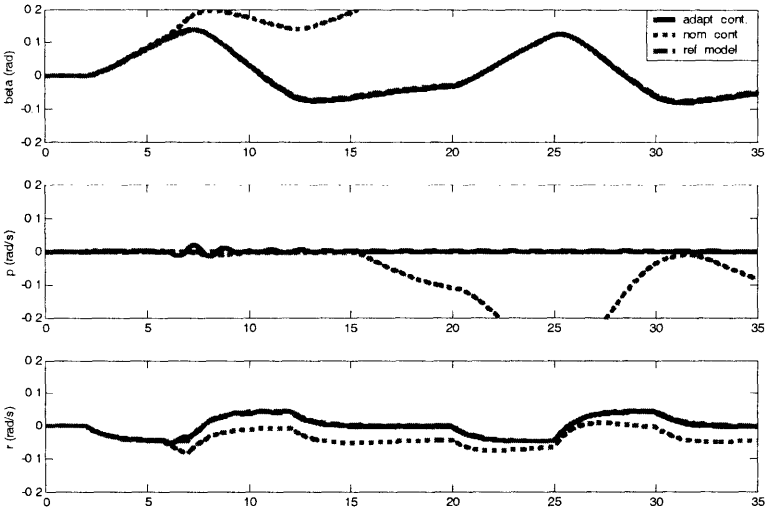

Figure 5-6: System response to failure 3, a failed left outboard engine giving zero thrust. The aircraft is commanded through two aggressive yaw doublets and the failure occurs at $t = 6s$. Only the lateral states are shown.

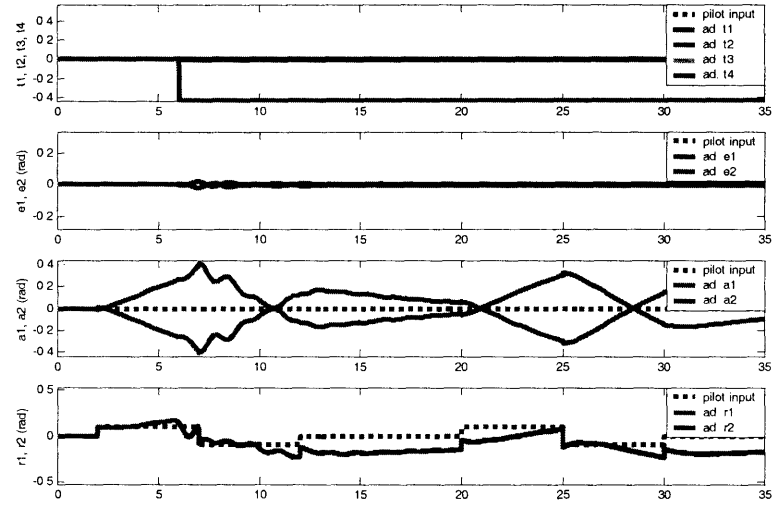

Figure 5-7: Actuator activity of the aircraft with failure 3, a failed left outboard engine giving zero thrust. The aircraft is commanded through two aggressive yaw doublets and the failure occurs at $t = 6s$

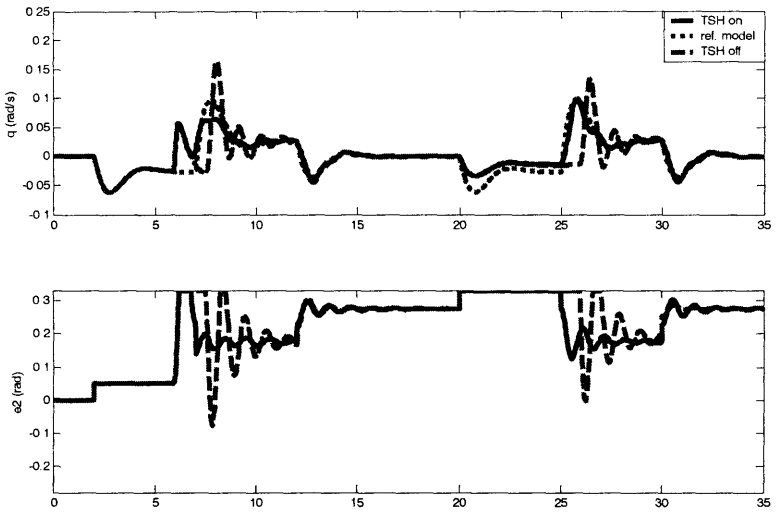

Figure 5-8: The stabilizing effect of TSH is illustrated for failure 4. The aircraft is commanded through two aggressive pitch doublets and the left elevator locks at 100% of its upward travel at $t = 6s$. Only the pitch rate and elevator activity are shown

For this case, the aircraft is commanded through two aggressive pitch doublets and the failure occurs at $t = 6$ seconds, as before. In comparison with failure 1, this failure provokes the actuators to saturate because the disturbance due to the locked actuator $f(5)$ is greater. The plots show the undesirable effects of saturation on the adaptive system without TSH. With TSH, the plant follows the model more closely, with less control activity. In this case the open loop plant was, in fact, stable, so stability is preserved despite the large saturation disturbance. An open-loop unstable plant will be more easily provoked to instability by saturation.

5.5 Summary

The problem of reconfiguration in the presence of actuator failures and saturation was considered in this chapter. A general linear model was formulated to adequately describe actuator failures of various types. An adaptive controller was proposed that incorporated two main improvements, which include an adaptive control allocation scheme and the use of a multi-input variation of TSH to preserve stability in the presence of saturation. It was proved in the previous chapter that the multi-input

TSH has bounded state trajectories for a set of initial conditions. The controller was compared to a fixed nominal controller in a simulation of a large transport aircraft with three different failures. The simulations demonstrated that the proposed controller can achieve stable reconfiguration following actuator failures in the presence of saturation. In addition to aircraft, the method proposed here is applicable to any dynamic system with multiple actuators capable of reconfiguration.

Chapter 6

Summary and Future Work

The tools and examples presented in this thesis are intended to form the beginning of an adaptive control verification and validation methodology for adaptive systems. First, we presented a simple set of procedures based on the RLAS to design adaptive systems to meet linear transient specifications. The RLAS tool was then demonstrated in two examples from flight mechanics; one involving uncertain linear short period dynamics with a nominal state feedback controller, the other involving a full, nonlinear, 6-DOF aircraft dynamics with a nominal LQ controller with integral action. Secondly, a tool was developed for controlling plants with magnitude saturation constraints on multiple inputs. The algorithm was shown to give bounded signals for initial conditions in a compact region, and was demonstrated in numerical simulation. Finally, a realistic design example was explored involving a linear aircraft model with uncertain dynamics and actuator failures. An adaptive controller was used for reconfiguration and control allocation. The controller was shown to give favorable response with uncertain dynamics, actuator failures and magnitude saturation.

Much work remains to be done to realize a practical V&V methodology, and the tools presented here must be further investigated and expanded to that end. For example, although not pursed in this thesis, the RLAS can be used as a tool to explore the effects of failures on the adaptive system dynamics. Uncertainties in the adaptive dynamics translate directly to uncertainties in the RLAS. The effect of these uncertainties on the RLAS can be straightforwardly investigated using the common

linear systems techniques, such as the root locus method, Bode plots, or Nyquist plots. Again, relying on the asymptotic convergence of the RLAS to the adaptive system, we can infer the effects of failures on the adaptive system response. Additionally, an analytically justified means of estimating the asymptotic gain error, θ_{xc}, should be investigated as the laborious task of iterating with simulation and control design to find appropriate values for Γ and Q is not sufficient in a practical setting.

Also, multi-input embodiments of the RLAS should be explored in conjunction with multivariable design techniques. One interesting extension of the RLAS design methodology is to use a cost function optimization to select adaptive parameters Γ and Q, thereby fusing the benefits of optimal and adaptive control. Such an extension ought to be easily within reach, and would automate the difficult and subjective multivariable adaptive control design task. In this vein, modifying current control design techniques to suit adaptive controllers will likely aid the transition of adaptive control technologies into aircraft and other safety critical applications in the future.

Finally, it was found in simulation that the algorithm for magnitude saturation compensation described in this thesis is also effective in compensating for rate saturation constraints, as well as combined rate and magnitude constraints, provided that a fast first order filter is applied to the control input rate, rather than a simple integrator. The evidence in simulation is compelling, however a formal proof of boundedness of signals has not been found for any open loop unstable case. Such a proof would bridge a precarious theoretical gap in the applicability of adaptive control to safety critical systems. Indeed, direct adaptive control with input rate constraints is an uncharted theoretical landscape.

The above research topics and others not mentioned here are currently underway toward integrating adaptive control with aircraft, automobiles, medical robotics and other safety critical applications. There is little doubt that adaptive control will find its uses in safety critical systems in the future, enhancing the reliability, autonomy, and simplicity of technologies on which we rely for our modern way of life.

Appendix A

Reconfiguration Simulation Values

Adaptive Gains:

$$\Gamma_i = 50 diag\left(\begin{bmatrix} 0.1 & 0.1 & 0.1 & 0.1 & 1 & 1 & 1 & 1 & 1 & 1 \end{bmatrix}\right), \text{ for } i = 1,2,3,4$$

$$Q = diag\left(\begin{bmatrix} 1 & 0.5 & 1 & 1 & 1 \end{bmatrix}\right)$$

Linearized Transport Aircraft Model:

$$A_p = \begin{bmatrix} -0.6582 & 0.9705 & 0 & 0 & 0 \\ -3.3105 & -1.4741 & 0 & 0 & 0 \\ 0 & 0 & -0.1706 & -0.0075 & -1 \\ 0 & 0 & -2.4792 & -1.3585 & 0.5897 \\ 0 & 0 & 0.8050 & 0.0559 & -0.5584 \end{bmatrix}$$

$$B_p = \begin{bmatrix} 0.0001 & 0.0001 & 0.0001 & 0.0001 & -0.0367 & -0.0367 & -0.0107 & -0.0107 & 0 & 0 \\ 0.0067 & -0.0011 & -0.0011 & 0.0067 & -1.8382 & -1.8382 & -0.0672 & -0.0672 & 0 & 0 \\ 0 & 0 & 0 & 0 & 0 & 0 & 0 & 0 & 0.0128 & 0.0128 \\ 0.0067 & 0.0038 & -0.0038 & -0.0067 & 0.1276 & -0.1276 & 0.5462 & -0.5462 & 0.0410 & 0.0830 \\ 0.1276 & 0.0726 & -0.0726 & -0.1276 & -0.120 & 0.0120 & -0.0620 & 0.0620 & -0.2366 & -0.02339 \end{bmatrix}$$

Reference Model:

$$A_m = \begin{bmatrix} -0.6582 & 0.9705 & 0 & 0 & 0 \\ -3.3105 & -1.4741 & 0 & 0 & 0 \\ 0 & 0 & -0.1706 & -0.0075 & -1 \\ 0 & 0 & 0 & 1 & 0 \\ 0 & 0 & 0 & 0 & -1 \end{bmatrix}$$

$$B_m = \begin{bmatrix} 0.0004 & -0.0734 & 0 & 0 \\ 0.0112 & -3.6764 & 0 & 0 \\ 0 & 0 & 0 & 0 \\ 0 & 0 & -1.0924 & 0 \\ 0 & 0 & 0 & -0.4705 \end{bmatrix}$$

Nominal Controller:

$$K_{nom_x} = B_a(B_pB_a)^+(A_m - A_p), \quad K_{nom_r} = B_a(B_pB_a)^+B_m,$$

where $(.)^+$ denotes pseudoinverse and where

$$B_a^T = \begin{bmatrix} 1 & 1 & 1 & 1 & 0 & 0 & 0 & 0 & 0 & 0 \\ 0 & 0 & 0 & 0 & 1 & 1 & 0 & 0 & 0 & 0 \\ 0 & 0 & 0 & 0 & 0 & 0 & -1 & 1 & 0 & 0 \\ 0 & 0 & 0 & 0 & 0 & 0 & 0 & 0 & 1 & 1 \end{bmatrix}$$

Initial Conditions:

$x(t_0) = 0$, $x_m(t_0) = 0$, $r(t_0) = 0$, $u_c(t_0) = B_a r(t_0)$, $K_x(t_0) = K_{nom_x}$, $K_r(t_0) = K_{nom_r}$, $\hat{k}_f(t_0) = 0$, $\hat{\lambda}(t_0) = \begin{bmatrix} 1 & 1 & 1 & 1 & 1 & 1 & 1 & 1 & 1 & 1 \end{bmatrix}^T$, $e_\Delta(t_0) = 0$.

Bibliography

[1] U.S. Dept. of Defense military specification: Flying qualities of piloted airplanes, November 5 1980.

[2] M. Bodson and J. E. Groszkiewicz. Multivariable adaptive algorithms for reconfigurable flight control. *IEEE Transactions on Control Systems Technology*, 5(2):217–229, March 1997.

[3] M. Bodson and W. A. Pohlchuck. Command limiting in reconfigurable flight control. In *Proceedings of AIAA Guidance, Navigation, and Control Conference*, New Orleans, LA, August 11 - 13 1997.

[4] D. J. Boskovic and R. K. Mehra. Multiple model adaptive flight control scheme for accommodation of actuator failures. *AIAA Journal of Guidance, Control, and Dynamics*, 25(4):712–724, July-August 2002.

[5] J. Burken, P. Lu, and Z. Wu. Reconfigurable flight control designs with application to the x-33 vehicle. In *Proceedings of the AIAA Guidance Navigation and Control Conference*, Portland, OR, 1999.

[6] H. Buus, R. McLees, M. Orgun, E. Pasztor, and L. Schultz. 777 fight controls validation process. *IEEE Transactions on Aerospace and Electronic Systems*, 33(2):656–666, 1997.

[7] A. J. Calise, S. Lee, and M. Sharma. Development of a reconfigurable flight control law for tailless aircraft. *AIAA Journal of Guidance, Control, and Dynamics*, 24(5), September-October 2001.

[8] J.-W. Cheng and Y.-M. Wang. *Adaptive Control of Nonsmooth Dynamic Systems*, chapter Adaptive Control For Systems with Input Constraints - A Survey, pages 311–332. Springer-Verlag, London, 2001.

[9] V. Cortellessa, B. Cukic, D. Del Gobbo, A. Mili, M. Napolitano, M. Shereshevsky, and H. Sandhu. Certifying adaptive flight control software. In *Proceedings of International Software Assurance Certification Conference*, Reston, VA, 2000.

[10] B. Cukic. The need for verification and validation techniques for adaptive control systems. In *Proceedings of International Symposium on Autonomous Decentralized Systems*, pages 297–298, 2001.

[11] E. L. Duke. V&V of flight and mission-critical software. *IEEE Software Magazine*, May 1989.

[12] W. C. Durham. Constrained control allocation. *AIAA Journal of Guidance, Control, and Dynamics*, 16(4):717–725, 1993.

[13] D. Enns. Control allocation approaches. In *Proceedings of the AIAA Guidance Navigation and Control Conference*, Boston, MA, 1998.

[14] R. A. Eslinger and P. R. Chandler. Self repairing flight control system program overview. In *Proceedings of IEEE National Aerospace and Electronics Conference*, volume 2, pages 504–511, 1988.

[15] Z. Gao and P. J. Antsaklis. On the stability of the pseudo-inverse method for reconfigurable control systems. *International Journal of Control*, 53(3):771–729, 1991.

[16] D. K. Henderson and E. Y. Lavretsky. Closed-loop model following and control allocation for transport aircraft using an ordered neural network-based approach. In *Proceedings of AIAA Guidance, Navigation, and Control Conference*, Portland, OR, August 9-11 1999.

[17] J. Hull and D. Ward. Verification and validation of neural networks for safety-critical applications. In *Proceedings of American Control Conference*, Anchorage, AK, 2002.

[18] J. James and D. Barton. A framework for verification and validation of integrated and adaptive control systems. In *Proceedings of IEEE International Symposium on Computer-Aided Control Systems Design*, Anchorage, AK, 2000.

[19] B. Jiang, J. L. Wang, and Y. C. Soh. An adaptive technique for robust diagnosis of faults with independent effects on system outputs. *International Journal of Control*, 75:792–802, July 20 2002.

[20] S. P. Karason and A. M. Annaswamy. Adaptive control in the presence of input constraints. *IEEE Transactions on Automatic Control*, 39(11):2325–2330, November 1994.

[21] K. S. Kim, K. J. Lee, and Y. Kim. Model following reconfigurable flight control system design using direct adaptive scheme. In *Proceedings of AIAA Guidance, Navigation, and Control Conference*, pages 995–1005, Monterey, CA, August 5-8 2002.

[22] J. P. LaSalle. Stability of nonautonomous systems. *Nonlinear Analysis: Theory Methods and Application*, 1:83–91, 1976.

[23] E. Lavretsky and N. Hovakimyan. Positive μ-modification for stable adaptiation in a class of nonlinear systems with actuator constraints. In *Proceedings of the American Control Conference*, volume 3, pages 2545–2550, Boston, MA, June 30 - July 2 2004.

[24] Y. Liu, S. Gururajan, B. Cukic, T. Menzies, and M. Napolitano. Validating an online adaptive system using svdd. In *Proceedings of IEEE International Conference on Tools with Artificial Intelligence*, Sacramento, CA, 2003.

[25] The Math Works. *MATLAB Optimal Control Tool Box Documentation.*

[26] R. V. Monopoli. Model reference adaptive control with an augmented error signal. *IEEE Transactions on Automatic Control*, AC-19(5):474–484, October 1974.

[27] K. S. Narendra and A. M. Annaswamy. *Stable Adaptive Systems*. Prentice Hall, Englewood Cliffs, New Jersey, 1989.

[28] H. Noura, D. Sauter, F. Hamelin, and D. Theilliol. Fault-tolerant control in dynamic systems: Application to a winding machine. *IEEE Control Systems Magazine*, 20:33–49, 2000.

[29] A. B. Page and M. L. Steinbergs. A closed loop comparison of control allocation methods. In *Proceedings of the AIAA Guidance Navigation and Control Conference*, Denver, CO, 2000.

[30] J. Renfrow, S. Leibler, and J. Denham. F-14 flight control law design, verification, and validation using computer aided engineering tools. Technical Report A762492, Naval Air Warfare Center, Aircraft Div., Patuxent River, MD, February 1995.

[31] M. Schwager and A. M. Annaswamy. Adaptation-based reconfiguration in the presence of actuator failures and saturation. In *Proceedings of American Control Conference*, Portland, OR, June 8-10 2005.

[32] M. Schwager and A. M. Annaswamy. Direct adaptive control of multi-input plants with magnitude saturation constraints. In *Proceedings of IEEE Conference on Decision and Control*, Seville, Spain, December 12-15 2005.

[33] M. Schwager and A. M. Annaswamy. Towards verifiable adaptive flight control for safety critical applications. In *Proceedings of AIAA Guidance, Navigation, and Control Conference*, San Francisco, CA, August 15-18 2005.

[34] J.-J. E. Slotine and W. Li. *Applied Nonlinear Control*. Prentice Hall, Upper Saddle River, New Jersey, 1991.

[35] B. L. Stevens and F. L. Lewis. *Aircraft Control and Simulation.* John Wiley and Sons, Inc., Hoboken, New Jersey, 2nd edition, 2003.

[36] D. A. Suarez-Cerda and R. Lozano. *Adaptive Control of Nonsmooth Dynamic Systems*, chapter Adaptive Control of Linear Systems with Poles in the Closed LHP with Constrained Inputs, pages 349–359. Springer-Verlag, London, 2001.

[37] G. Tao, S. M. Joshi, and X. Ma. Adaptive state feedback and tracking control of systems with actuator failures. *IEEE Transactions on Automatic Control*, 46(1):78–95, January 2001.

[38] C. J. Tomlin, I. Mitchell, A. M. Bayen, and M. Oishi. Computational techniques for the verification of hybrid systems. In *Proceedings of IEEE Conference on Decision and Control*, volume 91, July 2003.

[39] J. Virnig and D. Bodden. Multivariable control allocation and control law conditioning when control effectors limit. In *Proceedings of the AIAA Guidance Navigation and Control Conference*, Denver, CO, August 2000.

[40] J. M. Wohletz, J. D. Paduano, and A. M. Annaswamy. Retrofit systems for reconfiguration in civil aviation. In *Proceedings of AIAA Guidance, Navigation, and Control Conference*, pages 995–1005, Portland, OR, August 9-11 1999.